AUTOMATED METHODS FOR EVALUATING STORMWATER DRAINAGE SYSTEMS AT THE NEIGHBORHOOD SCALE USING MOBILE LIDAR DATA

A Dissertation

by

CHENG-CHUN LEE

Submitted to the Office of Graduate and Professional Studies of
Texas A&M University
in partial fulfillment of the requirements for the degree of

DOCTOR OF PHILOSOPHY

Chair of Committee,	Nasir Gharaibeh
Committee Members,	Francisco Olivera
	Ali Mostafavi
	Burak Guneralp
Head of Department,	Robin Autenrieth

May 2021

Major Subject: Civil Engineering

ABSTRACT

Assessing drainage conditions at the neighborhood level can help public works agencies to develop maintenance plans and mitigation strategies to guard against pluvial floods. Drainage condition assessments can also inform property owners about possible drainage problem areas. Current drainage condition assessment methods have two important shortcomings: (a) they depend on manual visual inspection, which is a time-consuming and labor-intensive process, and (b) they ignore areas outside the street right-of-way (e.g., adjacent front yards), despite the interdependency between public drainage system (e.g., roadside channel) and adjacent private properties. To address these shortcomings, this dissertation aims to develop automated methods for assessing the drainage conditions of roadside channels and adjacent land in residential areas by using mobile lidar (Light Detection and Ranging). Mobile lidar is increasingly used for evaluating infrastructure systems due to its ability to provide high-density and high-quality spatial measurements. This dissertation is organized into three technical papers. The first paper provides an automated process for inspecting and evaluating roadside channel systems using data obtained from mobile lidar. The Cloth Simulation Filtering algorithm was employed to split lidar point clouds into bare earth and object datasets. Six key geometrical attributes of roadside channels were computed and analyzed based on the bare earth dataset using statistical and heuristic methods. These geometrical attributes were compared to design and performance manuals to determine deficiencies and inform maintenance decisions. In the second paper, roadside topography was modeled to evaluate

surface drainage conditions by incorporating semantic segmentation and flow direction determination using mobile lidar data. The semantic segmentation model identifies the topographic features of lidar images by labeling each pixel as roadside channel, road, or adjacent land. Through the flow direction determination technique, major end points that are away from the roadside channels were identified as problematic low points that could be vulnerable to water ponding. In the third paper, the developed methods were applied to two communities in Harris county (Sunnyside community) and Aransas county (Rockport community) in Texas, with a total street length of 4.67 centerline miles. The six geometrical attributes for channel conditions and two attributes for off-channel conditions were evaluated and compared in the case studies. Overall, this dissertation shows that the developed automated process can evaluate roadside channels and model the roadside topography effectively. The developed methods provide actionable information to both property owners (to address potential off-channel ponding issues) and the municipal authorities (to address channel issues) to mitigate against localized flooding, water ponding, and stormwater-related hazards.

DEDICATION

To my dearest wife, Annie. Without you, none of this would have been possible.

Thank you!

ACKNOWLEDGEMENTS

I would like to thank my committee chair, Dr. Nasir Gharaibeh, for his advising and support in conquering every challenge through the journey. I also appreciate the guidance from my committee members, Dr. Francisco Olivera, Dr. Ali Mostafavi, and Burak Guneralp, toward my success. Besides, I am grateful to from Texas A&M Transportation Institute, especially Dr. Charles Gurganus, for providing critical supports to the success of my dissertation.

I want to extend my gratitude to my friends during this journey. The prayers and encouragement from the friends in Taiwanese Gospel Fellowship always put my mind at ease. Thanks also go to Feiyue Wang for his support and kindness when we both were all struggling. I would also like to thank those who chatted with me, played softball with me or sent encouraging texts to support me mentally and physically.

Finally, I deeply appreciate my family for their prayers and support.

CONTRIBUTORS AND FUNDING SOURCES

Contributors

This work was supervised by a dissertation committee consisting of Dr. Nasir Gharaibeh (advisor and committee chair), Dr. Francisco Olivera, and Dr. Ali Mostafavi of the Department of Civil and Environmental Engineering and Dr. Burak Guneralp of the Department of Geography.

The lidar data analyzed for the dissertation was collected by Dr. Charles Gurganus and Rick Canatella of Texas A&M Transportation Institute. Chapter 4 was written in part by Jessica Lee of the Department of Landscape Architecture and Urban Planning and Feiyue Wang of the Department of Civil and Environmental Engineering.

All other work conducted for the dissertation was completed by the student independently under the supervision of Dr. Nasir Gharaibeh.

Funding Sources

Graduate study was supported by a fellowship of International Texas Public Education Grant and a Teaching Assistantship during the 2020-2021 academic year.

TABLE OF CONTENTS

Page

LIST OF FIGURES

Page

LIST OF TABLES

Page

1. INTRODUCTION

1.1. Motivation and problem statement

Stormwater drainage systems are essential for collecting surface runoff and conveying it to discharge points to reduce the risk of flooding. Systematic evaluation of these systems provide a rational basis for developing flood management plans and mitigation strategies. The need for systematic inspection and evaluation of roadside channels has been emphasized in the literature (see for example (Frank & Falconer, 1990) to inform maintenance and improvement operations. Proper maintenance and upgrade of roadside channels ensure acceptable stormwater quality in the receiving streams, guard against localized flooding of adjacent streets and private properties, and protect the roadway structure (Brubaker, 2020). Similarly, the drainage conditions of roadside land affect the quality of stormwater, the risk of localized flooding, and the structural integrity of adjacent structures. Despite these calls, the evaluation and maintenance of roadside drainage systems (both channels and adjacent land) remain predominantly ad hoc because of the lack of efficient inspection methods, a critical gap in the literature.

Specifically, current drainage condition assessment methods have two common shortcomings: (a) they depend on manual visual inspection, which is a time-consuming and labor-intensive process, and (b) they ignore areas outside the street right-of-way (e.g., adjacent private properties or front yards), despite the interdependency between public drainage system (e.g., roadside channel) and the adjacent private properties. This research contributes to addressing these shortcomings through the development of a new automated method for the evaluation of roadside channels and adjacent land at the neighborhood

scale. The new method is based on data collected using mobile lidar (light detection and ranging) systems and novel algorithms for processing and analyzing these data.

Mobile lidar is increasingly used for evaluating infrastructure systems because of its ability to provide high-density and high-quality data about the geometry and surface type of surveyed objects rapidly (at traffic speed). For example, mobile land-based lidar has been utilized for creating preliminary drainage design at the project level (Gurganus et al., 2017), and identifying roadway surface type (Neupane & Gharaibeh, 2019), and various pavement evaluations, such as identifying pavement distress (Oliveira & Correia, 2009; Tsai & Chatterjee, 2018), evaluating pavement surface smoothness (Chin & Olsen, 2015), and assessing hydroplaning potential (Chou et al., 2017; Gurganus et al., 2017). This study extends the adoption of mobile lidar to the evaluation of drainage systems.

Because lidar systems collect large amounts of data, the processing of these data becomes a critical issue. This study contributes to the development of algorithms for processing and analyzing these data for drainage condition evaluation purposes. Three different techniques, namely, cloth simulation filter algorithm, semantic segmentation, and flow direction determination, are used to evaluate the condition of roadside drainage channels and adjacent land. Finally, the developed methods and techniques are applied to assess the drainage conditions in two Texas communities that are socially and physically vulnerable to flooding and stormwater-related hazards.

1.2. Research objectives

The aim of this study is to enhance the evaluation of drainage systems in residential areas through the automation of field surveys using mobile lidar and the processing and

analysis of the collected data. The dissertation is organized in three articles (each linked to a specific objective) that collectively demonstrate how this aim has been achieved. Three specific objectives and corresponding technical papers are presented as follows.

Objective #1: Develop an automated process for evaluating roadside channels by using mobile lidar data

Paper Title: *Automating the Evaluation of Urban Roadside Drainage Systems Using Mobile Lidar Data*

Paper Status: Published in *Computers, Environment and Urban Systems*, 2020.

Objective #2: Develop a computerized method for assessing surface drainage conditions in roadside channels and adjacent land

Paper Title: *Modeling Roadside Topography to Assess Drainage Conditions: A Computer Vision and Flow Direction Method Applied to Lidar Data*

Paper Status: Accepted for presentation at Transportation Research Board 2021. Paper has been submitted for publication in *Advanced Engineering Informatics*.

Objective #3: Assess the drainage conditions in Texas communities that are socially and physically vulnerable to flooding and stormwater-related hazards using automated methods

Paper: *Assessment of Stormwater Drainage Conditions in Socially and Physically Vulnerable Communities: Case Studies*

Paper Status: Accepted for presentation at ASCE International Conference on Transportation & Development (ICTD 2021). Paper will be submitted for publication in the International Journal of Disaster Risk Reduction.

1.3. Overview of papers

1.3.1. Paper 1: Automating the Evaluation of Urban Roadside Drainage Systems Using Mobile Lidar Data

Roadside channel systems are critical for the management of stormwater runoff and the protection of the structural integrity of roads; and thus, require systematic evaluation and maintenance. However, the evaluation of these systems remains ad hoc due to the lack of efficient inspection methods. This paper contributes to filling this gap by providing an automated process for the inspection and evaluation of roadside channel systems using data obtained from mobile lidar scanners. The Cloth Simulation Filtering algorithm was employed to split lidar point clouds into bare earth and object datasets, and then compute six key attributes of roadside channels based on the bare earth dataset. The six attributes are: channel depth, bottom width, side slope, longitudinal slope, and length and density of subsurface pipes and culverts. To test and demonstrate the new automated process, it was applied to six street sections in the City of Houston, Texas. The computed attributes were compared to the design and maintenance guidelines set by the City of Houston and Harris County. The evaluation results indicate that every channel examined in this study has its own condition issues and improvement needs. While no channel section in this study was in full compliance with the guidelines, no channel was utterly

incompatible either. The results show that the developed automated process can effectively and efficiently evaluate roadside channels, providing an alternative to conventional manual inspection methods.

1.3.2. Paper 2: Modeling Roadside Topography to Assess Drainage Conditions: A Computer Vision and Flow Direction Method Applied to Lidar Data

Local topography at the neighborhood and street scales affects the collection and convenience of storm runoff. Consequently, modeling local topography is critical for generating realistic water-flow simulations and evaluating the effectiveness of drainage systems. This paper provides a novel method for evaluating and modeling local topography at the neighborhood and street scales, enabling engineers to assess drainage conditions and take corrective maintenance actions more rapidly than currently possible. The developed method translates raw mobile lidar data, which are hard to interpret, into easily understood topographical properties by applying a semantic segmentation model (a computer vision technique) and flow direction model (a hydrology technique). The semantic segmentation (SS) model identifies the surface topographic features from lidar images (converted from point clouds) by labeling each pixel as roadside channel, road, or adjacent land. Fifty lidar images representing 50 street blocks in Houston, Texas were split into 30, 10, and 10 images for training, validating, and testing the SS model, respectively. Four SS models with different combinations of ResNet architectures and augmentation methods were trained on the basis of an Imagenet-1k pretrained model. Based on the test dataset, the selected model has intersection-over-union and accuracy values of about 80.3% and 88.5%, respectively. Flow direction, a common topographic index, was used

to determine surface flow conditions. Through the determination of flow direction, major end points that are away from the roadside channels were identified as problematic low points that could be vulnerable to water ponding. The surface drainage conditions of 10 street blocks (the test dataset) were evaluated using the proposed method. The results show that the proposed method can effectively model the roadside topography within a street block and compare it with that of other street blocks. The application of the proposed method can benefit both public works agencies and local residents by providing targeted information at the street and neighborhood levels so that improvements can be implemented in a timely manner to mitigate against localized flooding and water ponding.

1.3.3. Paper 3: Use of Mobile Lidar for Assessing Drainage Conditions in Residential Areas with Roadside Channels: Case Studies

Assessing drainage conditions of roadside channels and adjacent properties to ensure drainage capabilities at the neighborhood level is important in residential areas. The evaluation information can help government agencies to develop maintenance plans and mitigation strategies to protect against pluvial floods. The objective of this study is to assess the drainage conditions in two Texas communities that are socially and physically vulnerable to flooding and stormwater-related hazards using automated methods. The studies related to the evaluation of drainage systems in residential areas and the current drainage channel guidelines were reviewed to understand the most recent research and requirements. The evaluation methods proposed in previous studies were implemented in two study communities in Harris county (Sunnyside community) and Aransas county (Rockport community) in Texas, with a total street length of 4.67 centerline miles. Six

attributes for channel conditions and two attributes for off-channel conditions were evaluated and compared. The comparison of all evaluation attributes showed that the overall channel conditions in the Rockport community are relatively better than those in the Sunnyside community. The differences in channel conditions between the two communities may be attributed to the intensity of the developed lands and the age of the community. For off-channel drainage conditions, although both medians of the off-channel attributes in the Rockport community are less than that in the Sunnyside community, there are three relatively critical spots in the Rockport community that require improvement. Finally, the case studies show that mobile lidar data can be used to evaluate drainage systems and provide actionable information to both property owners (to address potential off-channel ponding issues) and the municipal authorities (to address channel issues).

2. AUTOMATING THE EVALUATION OF URBAN ROADSIDE DRAINAGE SYSTEMS USING MOBILE LIDAR DATA[1]

2.1. Introduction

Roadside channels are critical components of the roadway structure and the stormwater systems in urban areas. As a component of the stormwater drainage system, roadside channels play an essential role not only in the collection and conveyance of stormwater runoff to the downstream or natural rivers, but also in enhancing stormwater infiltration and improving water quality (Biesboer & Elfering, 2003). Thus, a properly designed and maintained roadside channel system can result in the delivery of less runoff and pollutants through runoff filtration and volume attenuation (K. Ellis et al., 2014). It is vital to ensure that roadside channels are maintained properly and systematically. Poorly maintained roadside channels may lead to lower water quality in the receiving streams, poor roadway surface drainage, weakened roadway structure, and flooding in adjacent properties (Brubaker, 2020). Therefore, many specifications and guidelines call for monitoring drainage channel conditions to inform maintenance activities. Generally, key drainage channel conditions include soil and vegetation issues, openness, profile, and geometry/dimensions (Arthur L. Storey, 1988; Haddock & Myers, 2018). The need for systematic inspection and evaluation of these systems has long been called for in the literature (Frank & Falconer, 1990). However, the evaluation and maintenance of these

[1] Reprinted with permission from "Automating the evaluation of urban roadside drainage systems using mobile lidar data" by Lee, C.-C., & Gharaibeh, N. G., 2020, *Computers, Environment and Urban Systems*, Volume 82, 101502, Copyright 2020 by Elsevier.

systems remain ad hoc due to the lack of efficient inspection methods, a critical gap in the literature.

Currently, drainage channel condition assessments are conducted using manual inspection methods with random sampling, which can be very time consuming and subjective, especially for quantitative measurements. Consequently, data on roadside drainage channels tend to be scarce, delayed, or even nonexistent (Oti et al., 2019). Oti et al. (2019) developed citizen-science methods to address this challenge for local communities. While that study found that volunteer citizen scientists can provide timely and high quality data on the conditions of drainage channels, they tend to have difficulties obtaining detailed quantitative measurements. This paper contributes to filling this gap by providing an automated process for the inspection and evaluation of roadside channel systems using data obtained from mobile lidar scanners. Specifically, we provide a method for automating the inspection and evaluation of channel profile and geometrical attributes to inform maintenance and renewal processes. New data processing techniques, including a point cloud filtering technique, are also presented in this paper.

Through the methods presented in this paper, critical measurements of roadside channels can be obtained efficiently, safely, and objectively. This critical information can help authorities to optimize maintenance and renewal activities. To test and demonstrate the new automated process, it was applied for six street sections in the City of Houston, Texas. The computed attributes were compared to the design and maintenance guidelines set by the City of Houston and Harris County.

2.1.1. Use of lidar technology in the domain of urban infrastructure systems

Mobile land-based lidar is increasingly being used for evaluating infrastructure systems because of its ability to provide high density and high-quality data. For example, vehicles equipped with lidar scanners have been used for various pavement evaluations, such as identifying pavement distress (Oliveira & Correia, 2009; Tsai & Chatterjee, 2018), evaluating surface smoothness (Chin & Olsen, 2015), determining drainage ability at the project level (Gurganus et al., 2017), identifying roadway surface type (Neupane & Gharaibeh, 2019), and assessing skid resistance (Chou et al., 2017). Lidar scanners installed on drones have been used to detect and determine geomorphic or linear features of suburban agrarian landscapes (Bailly et al., 2008; Passalacqua et al., 2012) and to detect builds and land use in urban areas (Bonczak & Kontokosta, 2019; Park & Guldmann, 2019; Weixing Zhang et al., 2017). This paper uses data obtained from a single unit land-based mobile lidar scanner to develop an automated process for the inspection and evaluation of roadside channel systems in urban settings. The developed process is more rapid and objective than current manual inspection methods.

2.2. Methodology

2.2.1. Cloth Simulation Filtering algorithm

Raw data from mobile lidar can contain extraneous information on surveyed areas that are irrelevant to the purpose of drainage system evaluation, such as trees, passing and parked vehicles, and mailboxes. This study uses the Cloth Simulation Filtering (CSF) algorithm, which employs a technique called cloth simulation (Weil, 1986), to filter out extraneous information and retain useful information only, such as channel profile and

geometry. By applying the CSF algorithm, points collected by mobile lidar are split into ground (bare earth) and non-ground (objects) datasets. The bare earth data was further analyzed in this study to calculate geometry-related channel attributes.

The CSF algorithm first inverts the lidar data and places an imaginary cloth above it. By dropping this cloth toward the inverted lidar data, the cloth can be deformed to fit the surface. Figure 2.1 shows an overview of the CSF algorithm. The final shape of the cloth is the imaginary terrain of the lidar data. Based on the actual difference between each point and the imaginary terrain, the point cloud of mobile lidar is split into two datasets, ground and non-ground. The CSF algorithm has six major user-defined parameters, which are grid resolution, time step, rigidness, steep slope fit factor, iteration number, and classification threshold. The definitions and values used in this study for these parameters are shown in Table 2.1.

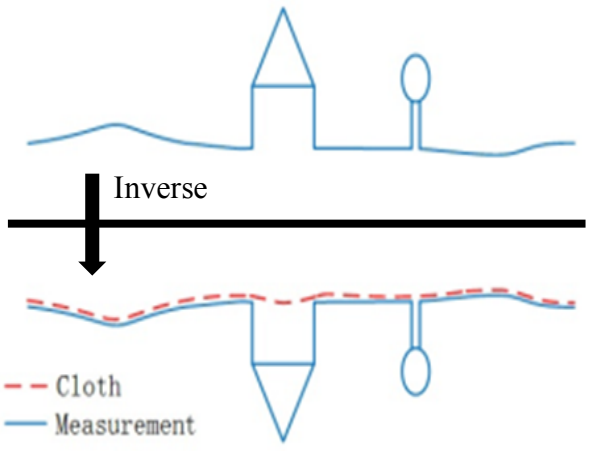

Figure 2.1 Overview of the CSF algorithm. [Adapted from Wuming Zhang et al. (2016)]

Table 2.1 Description of parameters for the CSF algorithm. [Adapted from Wuming Zhang et al. (2016)]

Parameter	Value used in this study	Definition
Grid Resolution	1 ft	Represents the distances among four neighboring particles of the cloth.
Time Step	0.5 s	Controls the displacement of particles during each iteration; the larger the time step, the more the movement is.
Rigidness	1	Controls the rigidness of the cloth; three preset rigidness values, from 1 to 3 represent from soft to rigid, respectively.
Steep Slope Fit Factor	TRUE	Indicates whether post-processing is required for handling steep slopes.
Classification Threshold	1 ft	The threshold for the distances between lidar points and the cloth grid; governs the final classification of the lidar points as bare earth or objects.
Iteration Number	500,000	The maximum number of iterations; termination marked by the maximum height variation of all particles being small enough or exceeding the maximum iteration number.

When applying the cloth simulation, the cloth is modeled as a grid, which consists of particles with mass and interconnections. To simplify calculations and improve efficiency, the CSF algorithm made three modifications toward the cloth simulation. First, particles are constrained to move vertically only. Second, as long as a particle reaches the ground, it becomes unmovable. Lastly, when dropping cloth to ground, the forces of each iteration are divided into two discrete steps. The particles of the cloth are firstly moved down owing to the gravity, and some of them may become unmovable when reaching ground. The second step is then modifying the position of the particles according to the internal forces. Grid resolution controls the distances among four neighboring points, and it is not ideal to be either too large or too small. A small grid resolution will decrease the

calculation efficiency and have overfitting issues. On the other hand, a large grid resolution may not be able to simulate the surface of the ground well. Time step and rigidness controls the movement caused by the gravity and the position adjustment caused by the internal forces, which are the first and the second steps when simulating forces. A post-processing procedure, steep slope fit, is applied to account for steep slopes that might not be captured from the previous simulation. Since the final cloth is at least equal or higher than the actual ground, the classification threshold provides a buffer to include more ground points; however, if the classification threshold is too large, more non-ground points will be included as well. Through an iterative process, the input values given in Table 2.1 were found to provide the best balance of these conflicting factors and thus are considered most suitable for the evaluation of urban roadside channels.

The source code for the CSF algorithm can be found on GitHub and author's website (Qi, 2020; W. Zhang et al., 2020). In this study, we tuned the CSF parameters to the values presented in Table 1 to obtain bare earth surfaces more accurately. Figure 2.2 shows a comparison of lidar data with and without applying the CSF algorithm. The objects that are irrelevant to drainage channel evaluations such as trees, grass, and the front walls of houses can be seen in the left of Figure 2.2. After applying the CSF algorithm, those objects were effectively removed. The remaining steps of the evaluation process use the bare earth surface, as shown in the right of Figure 2.2, which is free of irrelevant objects.

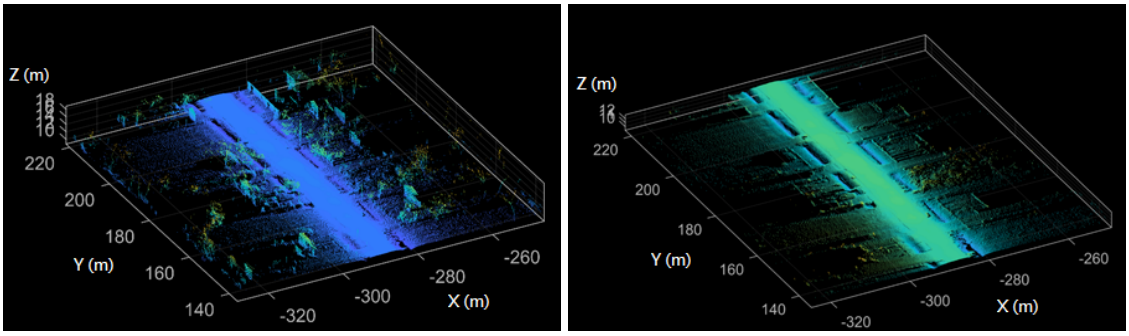

Figure 2.2 Comparison for mobile lidar data before (left) and after (right) applying the CSF algorithm.

2.2.2. Study site and mobile lidar data collection

This paper analyzes data collected using mobile lidar from neighborhoods in the City of Houston, Texas. These neighborhoods have a long history of flooding and environmental hazard issues. Figure 2.3 shows areas in the City of Houston, Texas that have roadside open-channel drainage systems, including the general location of the study site.

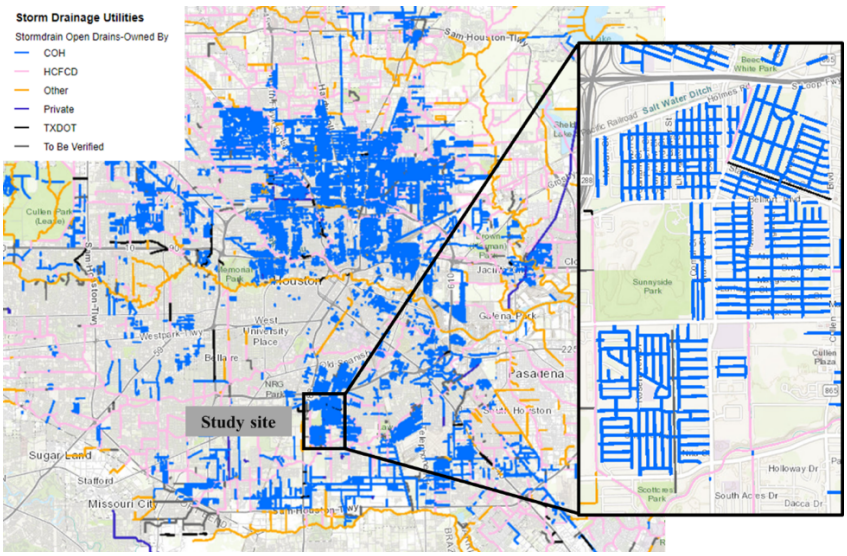

Figure 2.3 Open roadside drainage channels in the City of Houston. [Adapted from ("GIMS – Public Utility Map," 2020)]

A preliminary reconnaissance survey was performed on the entire neighborhood. Six street sections that were found to be representative of the neighborhood were selected for this study. The total street length of six street sections is approximately 10,000 feet. Figure 2.4 shows a schematic diagram of the study site configuration. For land-based mobile lidar data collection, laser proximity and the speed of the vehicle on which the scanner is mounted affect the point density of the lidar data. In this study, the lidar data had approximately 400,000 points per 0.1-mile section at a driving speed of 20 mph. Through data processing software, Road Doctor 3, point clouds of the study street sections were obtained and converted to data grids built on transverse and longitudinal increments of 2 inches. This grid size was selected to capture the smallest dimensional requirement of roadside channels in urban areas, which is the required channel's bottom width of at least 2 feet. (Arthur L. Storey, 1988; Haddock & Myers, 2018)

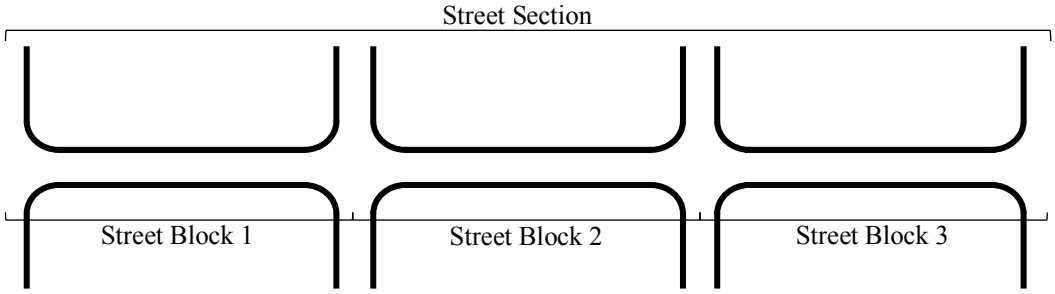

Figure 2.4 Schematic diagram of street sections and street blocks.

2.2.3. Design attributes for roadside channels

Many design guides and maintenance manuals set target values for key attributes as a basis for ensuring that roadside drainage channels operate effectively. However, the design requirements vary depending on the setting, such as highways, agricultural lands,

suburban areas, or urban areas. According to the infrastructure design manual published by the City of Houston (Haddock & Myers, 2018), the design of roadside channels in urban areas considers rainfall frequency, flow velocity, driveway and roadway crossings, and geometry limitations. These parameters control the channel system functionality. In this paper, six key attributes that affect the performance of roadside channels were selected and described in this section. Four of the six attributes are channel-related, which include channel depth, bottom width, side slope, longitudinal slope. Figure 2.5 is a schematic diagram showing the four channel-related attributes measured in this study. The other two key attributes are associated with subsurface pipes/culverts within the channel, which are the length and density of subsurface pipes/culverts. Their definitions, requirements, as described in the infrastructure design manuals of the City of Houston (COH) and Harris County (Arthur L. Storey, 1988; Haddock & Myers, 2018), and the calculation processes are explained below. The flowcharts for the calculation processes are provided in Appendix A.

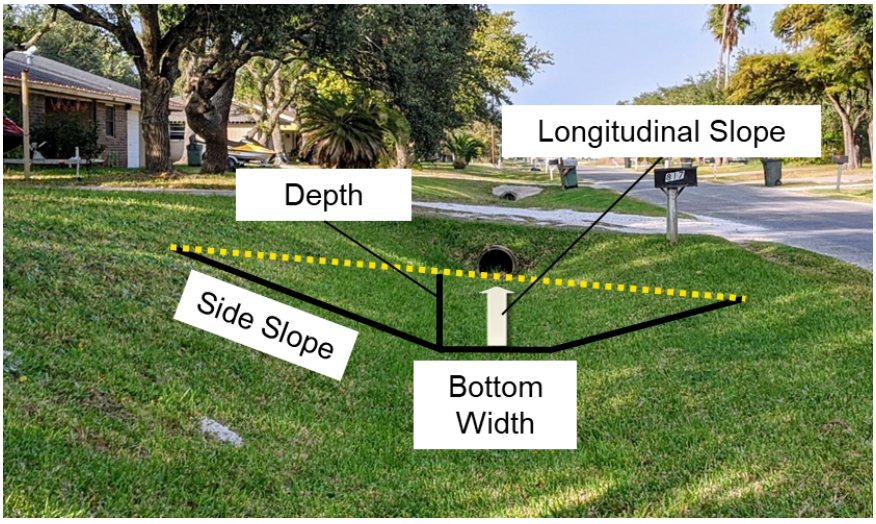

Figure 2.5 Schematic diagram for channel attributes.

2.2.3.1. Longitudinal profile preprocess

Channel grid data were extracted from the street sections and processed in three steps. First, for each channel, the lowest points transversely across the channel were identified and labeled as the profile of that channel (solid gray line in Figure 2.6), and the 300-foot moving average was calculated (black-dotted line in Figure 2.6). Second, for every three adjacent points, a critical point selection logic was developed to create upper and lower envelope lines (black and gray dashed lines in Figure 2.6). For generating the upper envelope line, if the second point was equal to or greater than the first and the third point, and larger than the moving average plus four inches, the second point was regarded as a critical point. By incorporating the moving average, the influence of irrelevant objects in drainage channels (e.g., debris) were avoided. An example of this situation occurs between 60 ft. to 100 ft. in Figure 6. Third, to make the envelope lines more accurate, two additional verifications for critical points were conducted after all critical points were selected. The critical point was removed from the upper envelope line if it was (a) the lower point of a critical point pair with a slope less than -0.05, or (b) the point connecting to two adjacent critical point pairs, of which slopes of both pairs were negative followed by positive slope and either slope had an absolute value greater than 0.05. A similar process was used for creating the lower envelope line, but the point identification logic was inverted. After all critical points were identified, the upper and lower envelope lines were drawn by linearly connecting those critical points. The data processing flowcharts for generating upper and lower envelop lines are shown in

Figure A. 1 and Figure A. 2 of Appendix A. The existence of surface channel was identified based on the lower envelope lines. If the difference between the channel profile point and the corresponding lower envelope line was less than or equal to four inches, the profile point was considered as parts of a surface channel (rather than subsurface pipes or culverts). Figure A. 3 shows the flowchart for identifying the existence of surface channels.

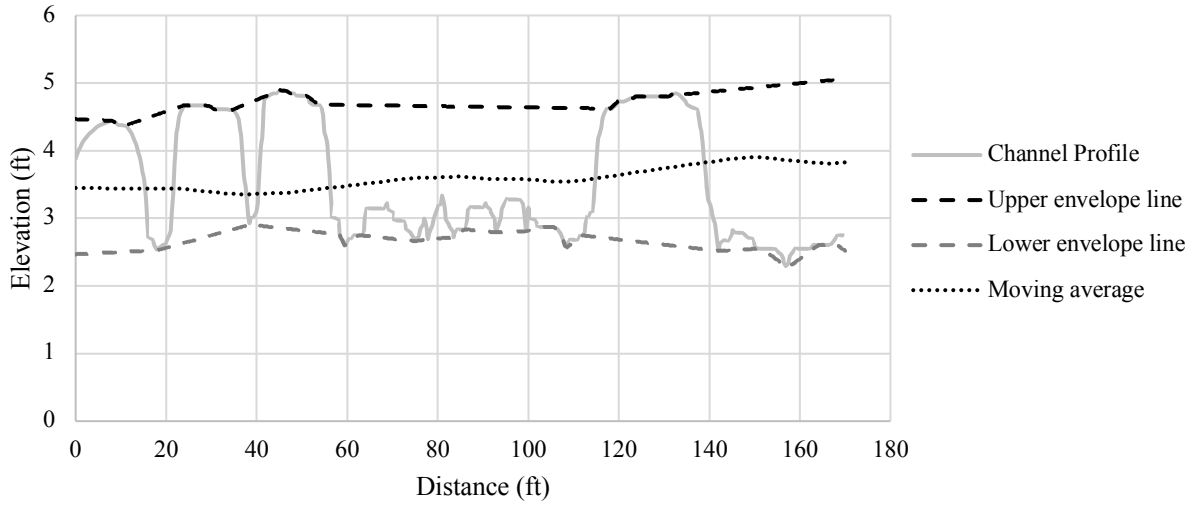

Figure 2.6 Schematic diagram for longitudinal profile development.

2.2.3.2. Channel depth

Channel depth affects its capacity. Based on the guidelines published by the City of Houston and Harris County, channel depth shall be at least the water depth to convey a minimum of 2-year rainfall and an additional minimum of 0.5 foot below the edge of pavement or the natural ground. Nevertheless, the minimum depth shall be 18 inches, and the maximum depth shall not exceed four feet. The channel depth was calculated as the difference between the two envelope lines. (Figure 2.7)

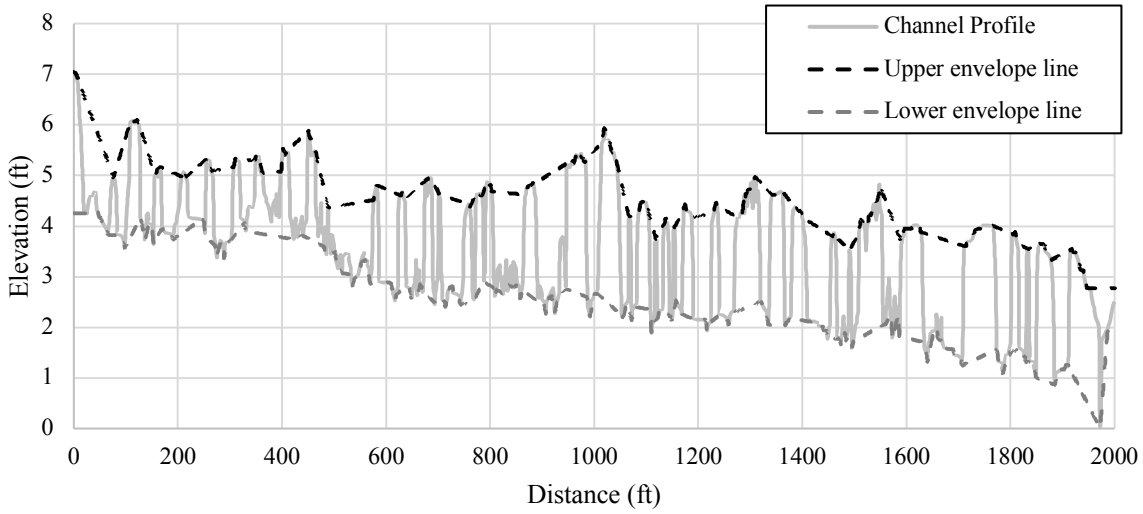

Figure 2.7 Example channel profile and the corresponding upper and lower envelop line.

2.2.3.3. Channel bottom width

The channel bottom width does not only affect the channel capacity but also influence hydraulic efficiency.(Service, 2008) The bottom width of a roadside channel is required by the City of Houston to be at least two feet wide. In this study, the bottom of a channel is determined as follows: all points adjacent to the channel profile point in the transverse direction, where open channels exist and are within an elevation difference of four inches. Therefore, the channel bottom width can be obtained by calculating the transverse distance across these points. The data processing flowchart for channel bottom width is shown in Figure A. 4.

2.2.3.4. Channel side slope

The side slope of a channel affects its stability and flow velocity. Local site conditions, such as soil type, surface treatment, maintenance method, and natural

topography, are the factors that determine the appropriate side slope value. Referring to the guidelines published by the City of Houston, the side slopes shall not be steeper than three horizontals to one vertical (3H:1V) for grass-lined or unimproved roadside channels. To calculate the side slopes, the boundary points of the side slopes must be determined first. In this study, the slopes of every transverse point pairs were first calculated. The boundary point identifying process started from the lowest point of each transverse line to compare adjacent slopes on both sides and stopped if the slope value is either less than or greater than zero two times in a row, depending on which side of the channel it is. As the boundary points of every transverse line are selected, the side slopes of the channel are calculated according to the bottom and the side boundaries of the channel. Figure A. 5 shows the data processing flowchart for calculating channel side slopes.

2.2.3.5. Channel longitudinal slope

The channel longitudinal slope significantly influences the velocity and the flow direction of the drained water. To avoid standing water, the City of Houston requires the minimum grade for roadside channels to be 0.1%. This study obtains the longitudinal slope of channels by calculating the slope of a linear regression line fitted to the channel bottom points within every street block. This method provides an overall indication of how the channel system performs in terms of water flow velocity and direction through street blocks.

2.2.3.6. Length and density of subsurface pipes and culverts

Due to the need for crossing roadside channels onto adjacent properties, subsurface pipes and culverts were often installed under driveways and streets. However, the drainage

capacities of subsurface pipes and culverts placed along channels are usually less than the channels themselves. Additionally, pipes and culverts are more prone to blockage than surface channels. Thus, the length and density of pipes and culverts are critical for the performance of channel systems. According to the driveway requirement of Harris County (Arthur L. Storey & Freeman, 2005), for single-family dwellings, the minimum and maximum driveway lengths are 16 and 40 feet, respectively. The length and density of pipes and culverts are determined based on whether open channels exist. Since some higher portions of profiles do not belong to either driveways or channel bottoms, further criteria are required to have more accurate identification for pipes and culverts. There are three different identification results based on point intervals between every two adjacent channel bottom points. If the point interval was greater than 20 feet, the two points are considered to be separated by a pipe or culvert. If it was less than one foot, the two points were determined to belong to the same surface channel. Otherwise, the 80^{th} percentile elevation of the points between two adjacent channel bottom points and the 20^{th} percentile elevation of the points belonging to the last identified channel were compared. If the difference between them was greater than eight inches, these two points are considered to be separated by a pipe or culvert. After the start and end points of each driveway within a channel were identified, the length and density of subsurface pipes and culverts were calculated. The flowchart for calculating the length and density of subsurface pipes and culverts is shown in Figure A. 6.

2.3. Results

The developed method was applied to six street sections in the City of Houston, Texas. The total length of these streets is approximately 10,000 feet, with continuous drainage channels on both sides of the streets. Thus, this study evaluated a total of 20,000 feet of roadside channels using the developed methods. Table 2.2 shows the length of each evaluated section.

Table 2.2 Evaluated street sections.

Section Number	1	2	3	4	5	6
Section Length (ft)	2,001.17	1,883.17	1,528.67	790.67	1,210.5	2,611.5

Section 4 is the only street that is shorter than 1,000 feet; however, with the exception of section 4, all of the other sections contain at least one intersection. That is, the length of every street block was around 1,000 feet. For each section, all six attributes were calculated according to the developed method and are discussed as follows.

2.3.1. Channel depth

Figure 2.8 shows the average channel depth (CD), and their standard deviations, for both the left and the right channels of each section in the study site. The right channel of Section 3 was the shallowest, and the right channel of Section 4 was the deepest among all sections. The right channel of Section 3 also had the smallest standard deviation of 0.095 feet, and the left channel of Section 4 was almost the same. On the other hand, the right channel of Section 6 had the highest standard deviation of 0.231 feet, which was two times more than the smallest standard deviation.

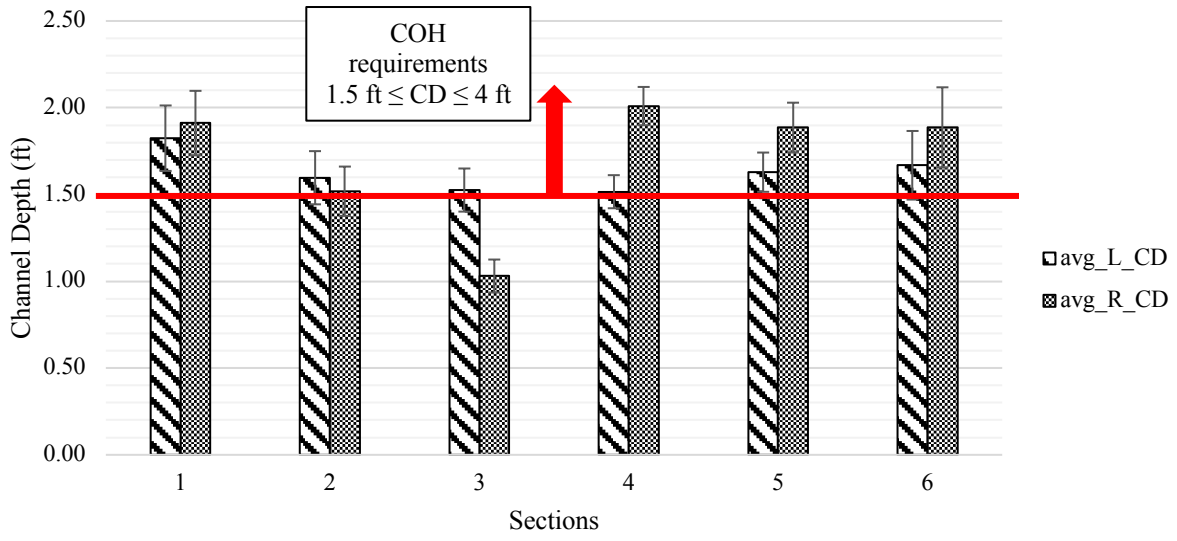

Figure 2.8 The average and standard deviation of channel depth.

According to the guidelines published by the City of Houston and Harris County, the channel depth should be between 1.5 and 4 feet. With the exception of the right channel of Section 3, which has an average depth of 1.0 feet, all channels have an average depth within the required range. Figure 2.9 shows the images of Sections 3 and 1 recorded during the lidar data collection. It can be seen that the right channel of Section 3 is shallower than the other three channels, which confirms these results. For six of the 12 channels, even the "mean plus one standard deviation" is within specifications.

Figure 2.9 Channel depth comparison between Section 3 (left) and Section 1 (right).

2.3.2. Channel bottom width

The channel bottom widths (CBW) for all study sections were calculated and shown in Figure 2.10. The average channel bottom width of the right channel of Section 3 was the widest among the 12 channels, and its standard deviation was also the largest. The right channel of Section 4 had the narrowest average bottom width and the smallest standard deviation.

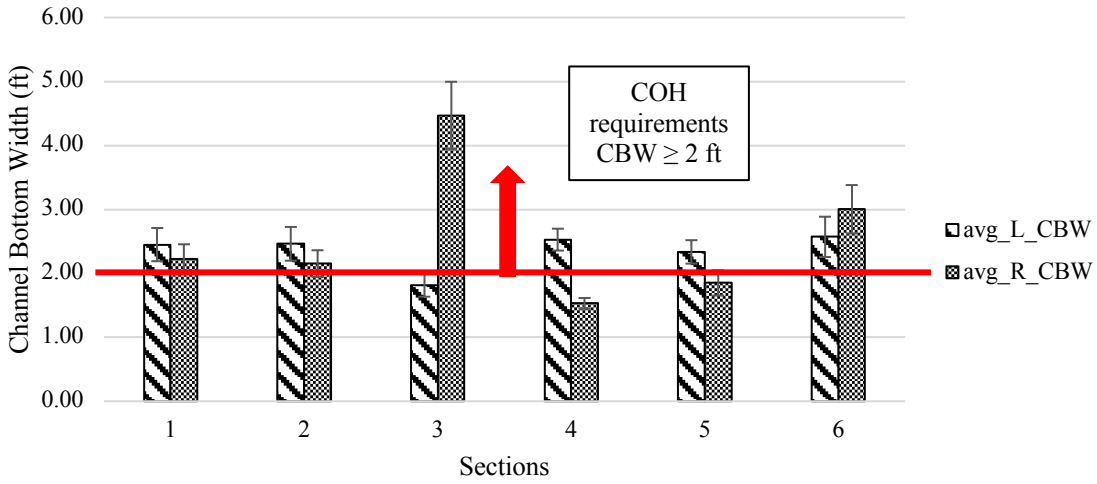

Figure 2.10 The average and standard deviation of channel bottom width.

The City of Houston requires that the channel bottom width be at least two feet wide. The average bottom width of three channels (out of 12) are less than two feet. These deficient channels are the left of Section 3 and the right of Sections 4 and 5. As shown in Figure 2.11, the right side channels of Sections 3 and 6 have a relatively flat bottom compared to the left side channels of Sections 3 and 6. For nine of the 12 channels, the "mean minus one standard deviation" bottom width is within specifications.

Figure 2.11 Channel bottom width comparison between Section 3 (left) and Section 6 (right).

2.3.3. Channel side slope

For easy understanding and comparison, the channel side slopes (SS) are shown by their absolute values in Figure 2.12. Each channel has two side slopes; that is, there were four side slopes for each street containing two channels. Of the evaluated channels, the left side slope of the right channel of Section 4 is the steepest (44%), and the left side slope of the right channel of Section 3 is the flattest (22%). The average channel side slopes for Section 6 are all flatter than the requirements. The differences among the standard deviations of all side slopes are relatively small.

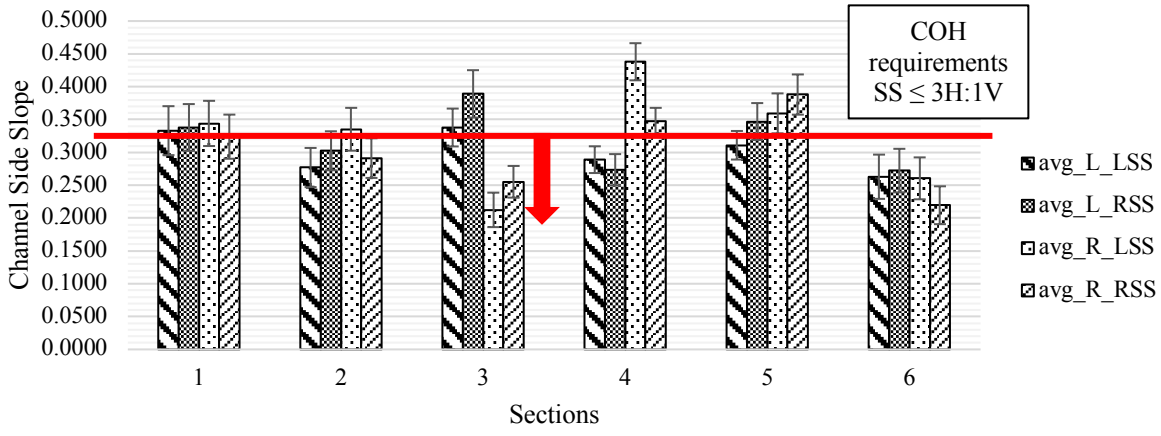

Figure 2.12 The absolute average and standard deviation of channel side slopes.

Since the streets selected in this study are grass-lined, the side slopes should not be steeper than three horizontals to one vertical (or 33%), based on the guidelines imposed by the City of Houston and Harris County. Fourteen average side slopes (out of 24) were not steeper than 33%. For 12 side slopes, the "mean plus one standard deviation" is within specifications. Figure 2.13 shows the channels in Sections 4 and 5, of which the average side slopes are steeper than the requirements except for the left side channel of Section 4.

Figure 2.13 Channel side slope comparison between Section 4 (left) and Section 5 (right).

2.3.4. Channel longitudinal slope

The channel longitudinal slope was calculated for each street block. As mentioned earlier, each section contained one to three street blocks. Table 2.3 shows the absolute longitudinal slope for each street block. The right channel of Street Block 1 in Section 5 has the highest longitudinal slope (0.444%), and the left channel of Street Block 3 of Section 6 has the flattest longitudinal slope (0.002%).

Table 2.3 Channel absolute longitudinal slope.

Section	Block	Left channel	Right channel
1	1	0.18%	0.19%
	2	0.24%	0.15%
2	1	0.12%	0.12%
	2	0.07%	0.04%
3	1	0.13%	0.17%
	2	0.17%	0.32%
4	1	0.12%	0.12%
5	1	0.11%	0.44%
	2	0.05%	0.03%
6	1	0.02%	0.05%
	2	0.19%	0.10%
	3	0.00%	0.14%

The City of Houston requires a 0.1% minimum grade for roadside channels to ensure water can flow downstream. The absolute longitudinal slopes of nine street blocks out of 24 were less than 0.1%, and one of them was near flat. In this paper, longitudinal slopes were calculated street block-by-street block, with the length approximately ranging from 550 ft. to 1,150 ft. A linear regression line may not be appropriate for longer street blocks with large variation in the profile. Generally, the inspection length for channel longitudinal slope should be established based on the variability of the profile, to ensure capturing high peaks and deep valleys that could affect the flow of water.

2.3.5. Length and density of subsurface pipes and culverts

Table 2.4 shows the lengths of subsurface pipes and culverts (P/C) as well as the P/C density (i.e., ratio of the accumulative length of pipes and culverts within a section to the length of the entire channel). The left channel of Section 5 had the highest pipes and

culverts density (53.44%); that is, more than half of the left roadside channel of Section 5 is under driveways.

In terms of the average length of pipes and culverts, no pipe or culvert was greater than 40 feet, which is the upper limit published by Harris County, but the pipes and culverts in the left channel of Section 5 and the right channel of Section 4 are near 40 feet.

Table 2.4 Length and density of subsurface pipes and culverts.

Section	Left channel		Right channel	
	Avg. length of P/C (ft)	P/C density	Avg. length of P/C (ft)	P/C density
1	24.32	38.89%	23.28	44.20%
2	21.11	43.71%	18.64	41.58%
3	27.27	48.17%	30.10	39.38%
4	21.59	35.50%	36.88	46.65%
5	38.05	53.44%	31.59	44.36%
6	22.35	33.38%	25.70	33.45%

*Density: ratio of total P/C length to total channel length

2.3.6. Condition ratings

After all attributes were calculated, an evaluation report can be generated for municipal authorities to plan maintenance and rehabilitation activities (Table 2.5). The report provides pass/fail ratings for each individual attribute of each section, as well as the overall picture of the condition of the channel system as a whole. By identifying the position of roadside channels, the automated evaluation process developed in this study converts raw lidar point cloud data to actionable information, as shown in the condition ratings.

Table 2.5 Condition evaluation report for six roadway sections.

Section	Side	Depth	Bottom Width	Side Slope(L)	Side Slope(R)	Lon. Slope	Avg. length of P/C	P/C density
1	L	P	P	P	F	P	P	38.89%
1	R	P	P	P	F	P	P	44.20%
2	L	P	P	F	F	F	P	43.71%
2	R	P	P	P	F	F	P	41.58%
3	L	P	F	P	P	P	P	48.17%
3	R	F	P	F	F	P	P	39.38%
4	L	P	P	F	F	P	P	35.50%
4	R	P	F	P	P	P	P	46.65%
5	L	P	P	F	P	F	P	53.44%
5	R	P	F	P	P	F	P	44.36%
6	L	P	P	F	F	F	P	33.38%
6	R	P	P	F	F	F	P	33.45%

2.4. Discussion

2.4.1. Channel system condition

Comparing the condition of channels with each other can provide an overview of how the channel system performs as a whole. Overall, the right channel of Section 3 is the shallowest with the widest bottom and the gentlest side slope (left side). The right channel of Section 4 has the deepest depth and the narrowest bottom width with the steepest side slope (left side). However, both channels do not fully meet the requirements set by the City of Houston; the right channel of Section 3 is too shallow, and the right channel of Section 4 is too narrow at the bottom.

No channel in the study site is in full compliance with the conditions required by the City of Houston and Harris County. For example, Section 6 performs well in terms of the channel depth, the bottom width, and average length of pipes and culverts on both sides, but the longitudinal slopes are substandard. Nevertheless, no channel is utterly

incompatible with the requirements set by the City of Houston and Harris County. Every channel in this study has its own individual issues for concern and improvement.

2.4.2. Individual channel condition

The lidar data are very detailed, allowing for evaluating conditions within each channel. Figure 2.14 shows the profile and the upper and lower envelope line of Section 3, as an example, which includes two street blocks split at 925 feet. As Figure 2.14 shows, the elevation of the lower envelope line between 400 and 900 feet is relatively small and flat, which means the channel within this range may have a higher opportunity to retain water, even though the longitudinal slope of the entire first street block is sufficiently high (0.13%). Additionally, the peak point of the elevation of the lower envelope line of the second block is in the middle of the block; that is, the channel drains water in two directions depending on the position of the channel. A single value of the longitudinal slope in Block 2, 0.174%, may mislead to a conclusion that the channel tilts to one direction and is relatively flat; however, the fact is if dividing Block 2 into two parts at 1,360 feet, the absolute slopes of these two parts are 0.322% and 1.863%, which are significantly greater than the composite value. This analysis shows that lidar data, combined with the process developed in this study, have the capability to evaluate roadside channels in an objective and automated manner.

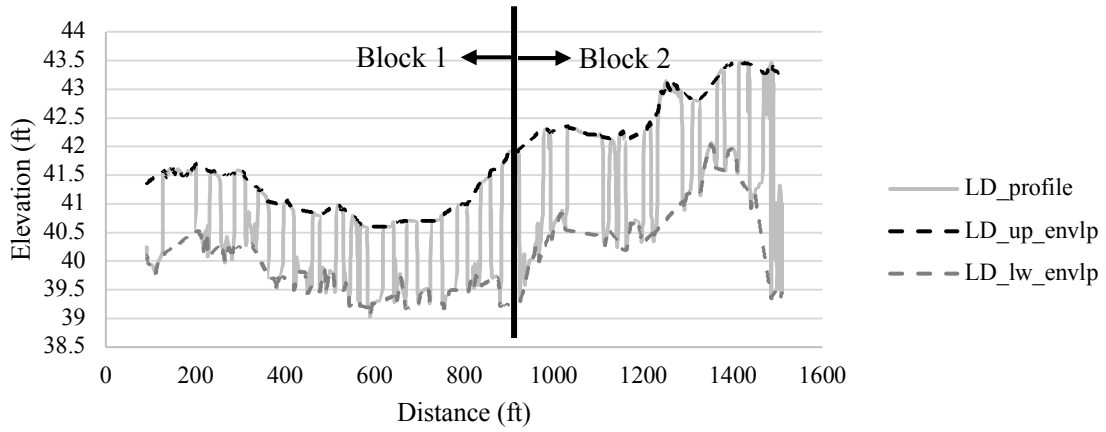

Figure 2.14 Profile and upper and lower envelope lines of the left channel of section 3.

2.5. Summary, conclusions and recommendations

Roadside drainage channel systems play an essential role not only in the collection and conveyance of stormwater runoff, but also in the enhancement of stormwater infiltration and water quality and the protection of the road structural integrity. This paper provides an automated method for the inspection and evaluation of roadside channel systems using data obtained from mobile lidar scanners. The Cloth Simulation Filtering algorithm was employed to split the lidar point clouds into bare earth and object datasets, and then compute six key attributes of roadside channels based on the bare earth dataset. The six attributes are: channel depth, bottom width, side slope, longitudinal slope, and length and density of subsurface pipes and culverts. These attributes can be compared to design and performance standards to inform maintenance decisions. This study collected lidar data on six street sections in Houston, Texas. The total length of these six street sections is approximately 10,000 feet with roadside channels on both sides of each street.

The developed automated process was used to evaluate the six street sections. The analysis results show that the channels in the study site are neither in full compliance nor utterly incompatible with the conditions required by the City of Houston and Harris County. Every channel was found to have its own individual own condition issues and improvement needs. For instance, the right channel of one street section met the depth requirement, but it did not meet the bottom width requirement. On the other hand, the right channel of another section has the opposite conditions. While no channel section in this study was in full compliance with the guidelines, no channel was utterly incompatible either. The results show that the developed automated process can effectively and efficiently evaluate roadside channels, providing an alternative to conventional manual inspection methods. Since mobile lidar can capture nearly continuous measurements along the channel, this study shows the potential for evaluating channels at shorter sections to inform targeted improvements and maintenance.

Finally, further studies would be needed in four areas: a) determine the optimal length of the evaluation section to ensure capturing variations in the channel's profile that could affect water flow (i.e., high peaks and deep valleys), b) relate the condition of channels to the risk of flooding to inform both the municipal government and property owners about effective mitigation measures, c) investigate the advantages and disadvantages of land-based mobile lidar compared to airborne lidar for the inspection of roadside drainage channels, and d) integrate the developed methods and techniques into a unified tool.

3. MODELING ROADSIDE TOPOGRAPHY TO ASSESS DRAINAGE CONDITIONS: A COMPUTER VISION AND FLOW DIRECTION METHOD APPLIED TO LIDAR DATA

3.1. Introduction

Local topography affects the collection and conveyance of storm runoff to a stream, a river, or a discharge point. Consequently, modeling local topography (e.g., neighborhood scale) is critical for generating realistic water-flow simulations (Hackl, Adey, & Lethanh, 2018; Hackl, Adey, Woźniak, et al., 2018) and evaluating the effectiveness of drainage systems, which is a key factor for urban flood control (Xu et al., 2015). Often, however, there is no up-to-date and adequately detailed topographical information at the local level (e.g., catchment, neighborhood, or street scale). Furthermore, collecting such information is typically performed manually using conventional surveying methods or visual inspections, which are generally time-consuming and cost-prohibitive (Gao & Elzarka, 2021; Koch et al., 2015). This paper contributes to overcoming these challenges by providing a novel method for evaluating and modeling the topography of drainage systems at the neighborhood and street scales, enabling engineers to assess drainage conditions and take corrective maintenance actions more rapidly than currently possible. The developed method translates raw data from land-based mobile lidar (light detection and ranging) systems, which are hard to interpret, into easily understood topographical properties by applying a semantic segmentation (SS) model (a computer vision technique) and a flow direction model (a hydrology technique). The SS model was trained to identify roadside channels, road surface, and adjacent land surface from lidar

images converted from point clouds. Then, the output of the SS model was used in a flow direction model, which provides insights on how water is conveyed on the basis of digital elevation models (DEM).

The remainder of this paper is organized as follows: In the next section, an overview of the literature on lidar and computer vision within the context of infrastructure condition assessment and flood risk analysis is provided. The section titled "Methodology" describes both the SS model and the flow direction model. Then, the results obtained from applying the methodology to street blocks in the Houston, Texas area are discussed. Finally, the research summary and conclusions are presented.

3.2. Literature review

Mobile lidar is increasingly being used for inspecting infrastructure systems because of its ability to provide high-density and high-quality data at traffic speed. For example, mobile lidar has been used in bridge inspections (Bolourian & Hammad, 2020; G. Cha et al., 2019; Gargoum et al., 2018), pavement inspections (Chou et al., 2017; Gurganus et al., 2017; Oliveira & Correia, 2009), and building detection (Zhou & Gong, 2018). This study uses mobile lidar data to evaluate surface topography and drainage conditions at the street and neighborhood scales.

Research on modeling roadside topography has been limited since most of existing surface flow models focus on large-scale networks and areas (J. B. Ellis et al., 2012). Only a few studies have modeled surface flows in local areas using mobile lidar data. Ettrich et al. (2005) proposed a method for modelling surface runoff and sewer flow in urban areas by using airborne lidar data and incorporating sewer system information. However, that

method may have missed the area's complex details because of the relatively low resolution of airborne lidar data. To obtain a more reliable and accurate flood risk analysis, J. B. Ellis et al. (2012) used a combination of airborne and terrestrial lidar to collect detailed topographical data at the neighborhood level. However, the analysis requires additional inputs on the sewer and drainage networks beyond the lidar data. Thus, a critical gap in the literature is to identify problematic low points and areas that could lead to poor drainage at the street and neighborhood levels by using lidar data only. This paper contributes to addressing this gap using computer vision and flow direction techniques applied to lidar data.

Computer vision and deep learning techniques are increasingly implemented in infrastructure condition assessments and identification of infrastructure elements from images. Among these applications, crack detection is one of the most prevailing applications in civil engineering. Several studies (Y.-J. Cha et al., 2017; Dung & Anh, 2019; Kalfarisi et al., 2020; B. Kim & Cho, 2019; X. Zhang et al., 2019) applied deep convolutional neural networks (CNN) to concrete crack detection by proposing different model architectures or loss functions to determine the characteristics of concrete cracks. Aside from crack detection, pavement distress detection is also prevalent. Several studies (Gopalakrishnan et al., 2017; Maeda et al., 2018; K. Zhang et al., 2018) trained deep CNN models to detect various types of road damages based on images. In addition, Zhou and Gong (2018) developed a deep neural network to recognize and extract residential building objects from airborne lidar data without providing any pre-defined geometric or texture features. Atkinson et al. (2020) and Czerniawski and Leite (2019) used mask-RCNN and

semantic segmentation to identify different indoor components to create annotated records for building asset management. Nath and Behzadan (2019) proposed a deep CNN model to retrieve labor-intensive task information, such as safety inspection and crew activity logs, from images or videos of construction sites. In this study, we used semantic segmentation, a computer vision technique, for labelling lidar image pixels into classes. Semantic segmentation has been used previously in autonomous driving (Cordts et al., 2016), concrete crack detection (Dung & Anh, 2019; X. Zhang et al., 2019), indoor infrastructure labeling (Czerniawski & Leite, 2019), and indoor navigation (W. Kim & Seok, 2018). While computer vision has been used in several areas within civil engineering, its application for drainage condition assessment remains limited. In this study, semantic segmentation was applied to land-based mobile lidar data to identify different roadside drainage features. The output of this model is then used in a flow direction model to identify problematic low points and areas.

3.3. Methodology

Two techniques from computer vision and hydrology were integrated to model local topography and assess surface drainage conditions in residential areas. The two methods are described in the following sections.

3.3.1. Semantic segmentation

Fully convolutional networks (FCN) (Long et al., 2015) is a method for solving sematic segmentation problems (Kirillov et al., 2019). FCN takes advantage of existing CNN classification models and transforms them into fully convolutional models by replacing the fully connected layers with spatial maps (Garcia-Garcia et al., 2017). FCN

shows that CNN can be trained end-to-end for semantic segmentation problems with various input sizes. Two prominent directions based on FCN for improving prediction performances are DilatedFCN and encoder-decoder methods (H. Wu et al., 2019). Several studies on DilatedFCN (L. Chen et al., 2018; L.-C. Chen et al., 2017; Yu & Koltun, 2015; Zhao et al., 2017) utilized dilated convolution, as known as atrous convolution, to increase feature resolution by keeping receptive fields. However, this approach can substantially increase computation load and memory consumption (Zhao et al., 2017). By comparison, encoder-decoder methods (Badrinarayanan et al., 2017; Lin et al., 2017; Ronneberger et al., 2015) use an encoder to extract multilevel feature maps and then upsample by combining both high- and low-level feature maps to classify images.

In this study, a python package, namely, Detectron2 from Facebook AI Research (Y. Wu et al., 2019) was employed to conduct semantic segmentation model training. This package (Y. Wu et al., 2019) adopts an encoder-decoder framework called Feature Pyramid Network (FPN). FPN uses a lightweight decoder instead of a symmetric decoder like U-Net (Kirillov et al., 2019). For this semantic segmentation technique, feature maps from different scale levels of the FPN pyramid are merged into a single output. For the deepest FPN level at 1/32 scale, the upsampling process, which consists of convolutions and bilinear upsampling, is conducted three times to generate a feature map at 1/4 scale. The same strategy is repeated for each FPN level until each of them reaches 1/4 scale. The outputs from each FPN level are then summed and upsampled to generate pixel-wise outputs at the original image resolution. When this FPN semantic segmentation method was compared with other methods, Kirillov et al. (2019) concluded that this lightweight

and straightforward architecture is robust and provides a strong baseline for semantic segmentation. Hence, the present study adopted this semantic image segmentation model.

3.3.2. Flow direction

Flow direction is one of the most common topographic indices derived from gridded DEM, and is also needed for water path determination. The flow directions to a cell are assigned using the elevations of its eight neighboring cells to derive the local slope gradient from DEM (Qin et al., 2007). Several studies on flow routing algorithms are usually distinguished by single and multiple flow-direction algorithms (Wilson, 2018). The D8 algorithm (O'Callaghan & Mark, 1984), a single flow-direction algorithm, is the earliest and simplest method for specifying flow directions. The flow of a cell of interest is routed into one of its neighboring eight cells with the steepest slope. The advantage of D8 algorithm is easy to understand and apply due to its simplicity. However, the D8 algorithm may assign the discretized flow into only one of eight directions, and the flows tend to become concentrated to artificial straight lines (Seibert & McGlynn, 2007; Tarboton, 1997). In contrast to single flow-direction algorithms, multiple flow-direction (MFD) algorithms route water into one or more downslope cells. Quinn et al. (1991; 1995) proposed the MFD algorithm for distributing flows to all downslope neighboring cells in proportion to the slope toward that neighbor. The MFD algorithm addresses the limitation of the D8 algorithm; however, assigning flow with the former from one cell to two or more cells leads to the inherent problem of dispersion. Tarboton (1997) proposed the D-inf algorithm to minimize the effects of dispersion and retain the simple features of the D8 algorithm.

The D-inf algorithm (Tarboton, 1997) assigns flows to only one direction but can be any between 0 and 2π. As shown in Figure 3.1, flow direction is determined by the direction of the steepest downslope on the eight triangular facets formed in a 3 × 3 window. Thus, the flow of a cell can be assigned to one or two downslope cells in proportion to the closeness of the flow angle to the direct angle. In Figure 3.1, for example, the flow of cell B2 will be distributed to cells B1 and C1 because the steepest downslope direction is located in the second facet. The distribution of the flow is based on the angles α and β. This study used a MATLAB toolbox, TopoToolBox (Schwanghart & Scherler, 2014), for determining flow directions; which are then used to assess surface drainage conditions.

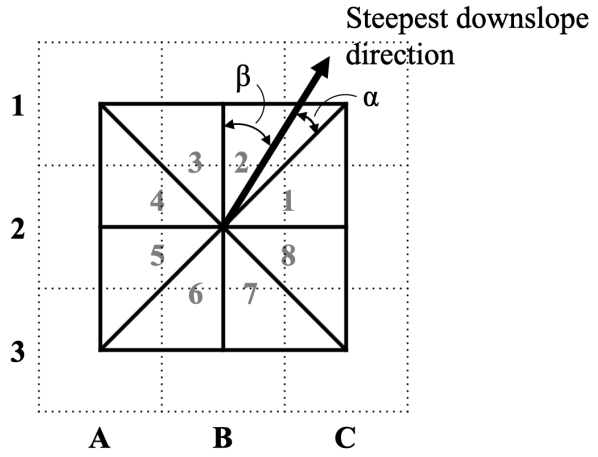

Figure 3.1 Schematic for identifying flow direction according to the steepest downward slope. [Adapted from Tarboton (1997)]

3.4. Data preparation

Land-based mobile lidar data were collected from two communities in east Texas. The first one is located in Houston and the second one is located nearby Rockport City. In this study, the lidar data had approximately 400,000 points per 0.1-mile section and were

collected at a driving speed of 20 mph. Raw lidar data can contain information irrelevant to the assessment of surface drainage conditions. Therefore, the lidar point clouds were first filtered to ground and non-ground datasets by using the Cloth Simulation Filtering (CSF) algorithm (Wuming Zhang et al., 2016). The CSF algorithm applies an imaginary cloth to the inverted point cloud as a filter boundary to separate points into ground or non-ground datasets. This study adopted the parameters of the CSF algorithm tuned in a related research that evaluated roadside channels (Lee & Gharaibeh, 2020). A before and after comparison is shown in Figure 3.2 to demonstrate the effect of the CSF algorithm. The bare earth point cloud datasets were filtered out and divided by street blocks. The point clouds of each street block were then converted to data grids built on transverse and longitudinal increments of two inches with natural neighbor interpolation. Fifty street blocks with a total length of about eight miles were collected from the two study sites.

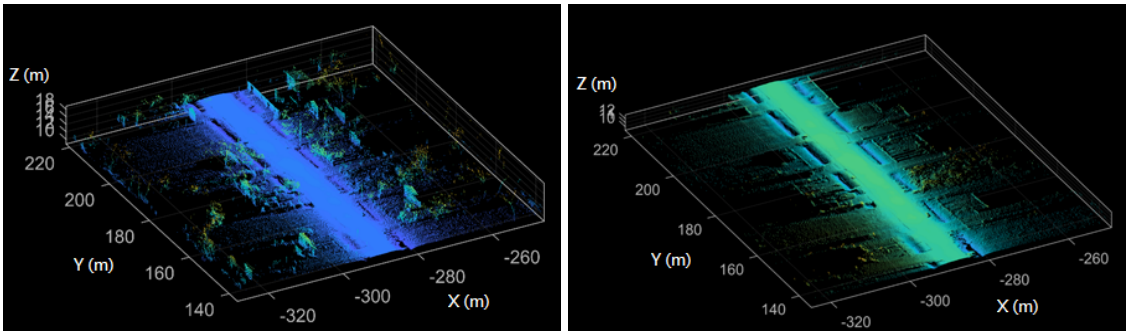

Figure 3.2 Comparison of lidar point cloud data before (left) and after (right) the CSF algorithm was applied. [Adapted from Lee and Gharaibeh (2020)]

The fifty street blocks were split into training, validation, and test datasets that contained 30, 10, and 10 randomly selected street blocks, respectively. Within each street block, each and every pixel was assigned to one of five labels, namely, “Roadside channel”, “Road”, “Adjacent Land”, “No data”, and “Not applicable”, by using Labelbox

(Labelbox, 2020). “No data” means the specific cell had no lidar point during the conversion of point clouds to grid data. “Not applicable” represents areas where only a few lidar points were present or areas affected by undesired objects that were not completely removed by the CSF algorithm. This label usually covers areas with buildings or trees. “Roadside channel” refers to areas with channels beside a street. “Adjacent land” denotes areas between “Not applicable” and “Roadside channel”. “Road” indicates street areas within a street block, and it is most likely at the center of the image. An example of a street block with assigned labels and its corresponding lidar data are shown in Figure 3.3. Fifty street blocks were processed and prepared accordingly for further analysis.

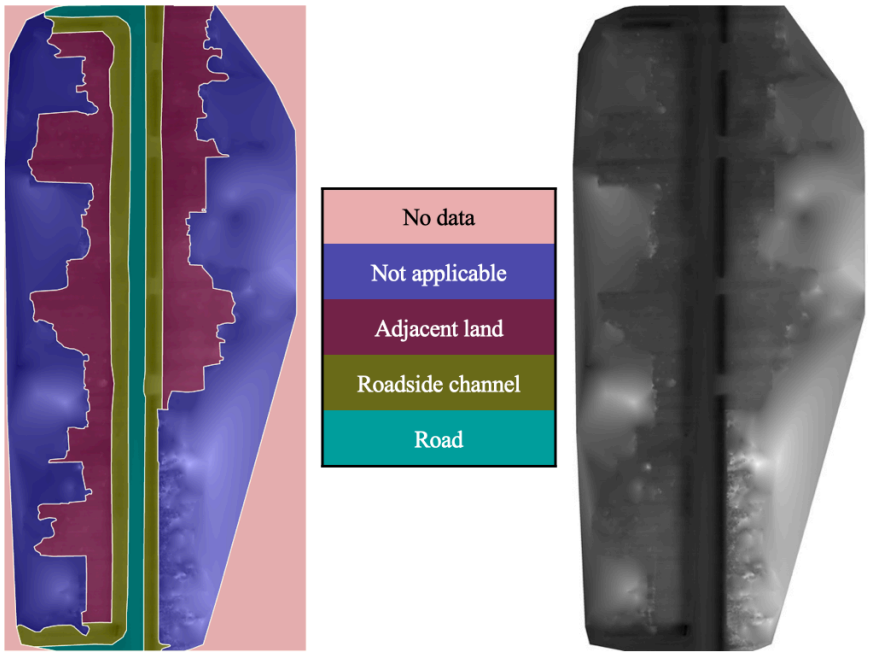

Figure 3.3 Example of a street block with assigned labels and its corresponding lidar data.

3.5. Semantic segmentation model training

Semantic segmentation was used to identify "Roadside channel", "Road", "Adjacent Land", "No data", and "Not applicable" areas within a street block. Given that the size of the lidar dataset was relatively small, transfer learning was implemented. The training results of the four models trained with ResNet-50 and ResNet-101 and pretrained on ImageNet-1k dataset are presented in this section. The ImageNet-1k dataset (Krizhevsky et al., 2012) had 1,000 categories and collected roughly 1,000 images per category; over 1.2 million images were used by the pretrained models. Data augmentation was also applied during training to improve the performance of the models. Three data augmentation methods, namely, random flipping, random resizing, and random cropping, were used. Table 3.1 presents the details of the architectures and augmentation methods used in each training model.

Table 3.1 Details of the architectures and parameters used in each training model.

Model	Backbone Architecture	Augmentation*
1	ResNet-50	RF, RR
2	ResNet-50	RF, RR, RC
3	ResNet-101	RF, RR
4	ResNet-101	RF, RR, RC

*RF: Random flipping, RR: Random resizing, RC: Random cropping

The models were trained by minimizing cross-entropy loss function, a popular and influential loss function that was designed to minimize the difference between ground truth and prediction by tuning the weights in networks (Krizhevsky et al., 2012). Four commonly used metrics were included, namely, pixel accuracy (pACC), mean pixel accuracy averaged across classes (mACC), mean Intersection-over-Union averaged across classes (mIoU), and frequency weighted Intersection-over-Union (fwIoU) (Caesar et al.,

2018). Figure 3.4 shows the training loss and validation loss of the four models up to 8,000 epochs. The results of the evaluation metrics calculated from the validation dataset are shown in Figure 3.5.

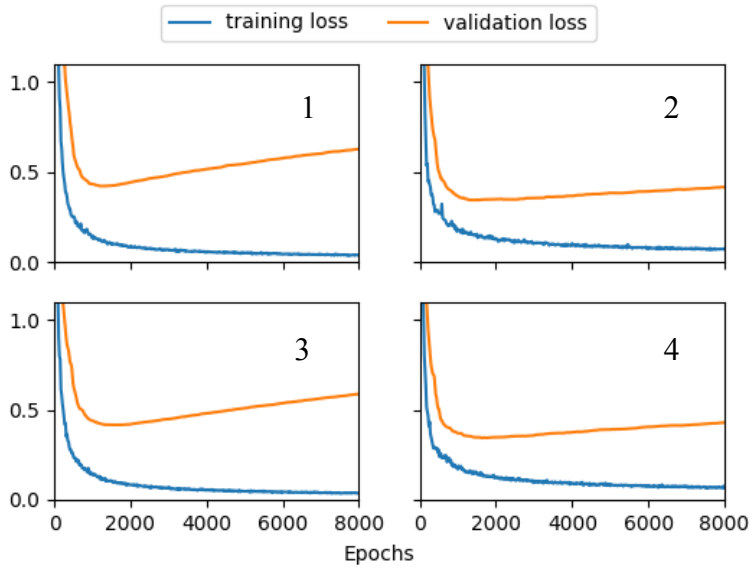

Figure 3.4 Training loss and validation loss of models 1, 2, 3, and 4 during training.

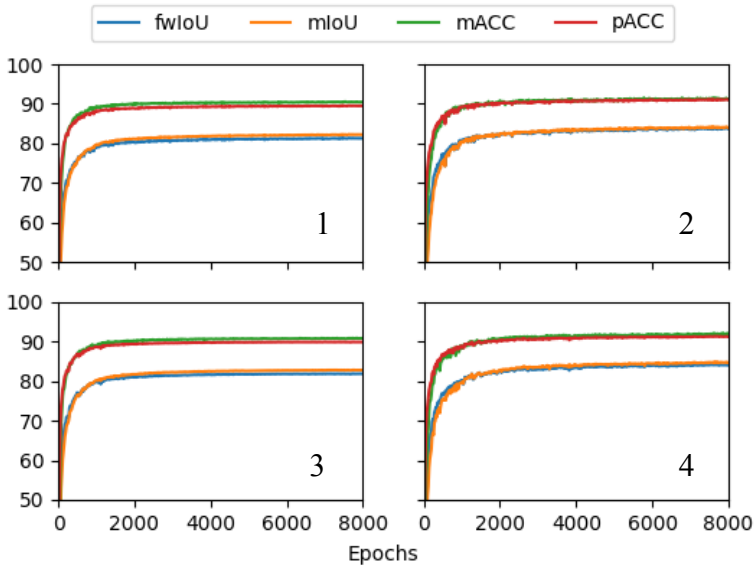

Figure 3.5 Evaluation metrics based on the validation dataset for models 1, 2, 3, and 4.

The validation loss of the four models stopped decreasing after approximately 1,000 epochs, and the evaluation metrics remained almost constant after about 2,000 epochs. At 2,000 epochs, the mACC and pACC of the four models approached or exceeded 90%, indicating that about 90% of the grids were correctly labeled. Moreover, the mIoU and fwIoU of the four models were above 80%, which was higher than 70%, a commonly used criterion to ascertain correct object detection. Therefore, the models trained with 2,000 epochs were chosen due to relatively good performance and avoid overfitting, and the models were tested by the test dataset. The test results are shown in Figure 3.6.

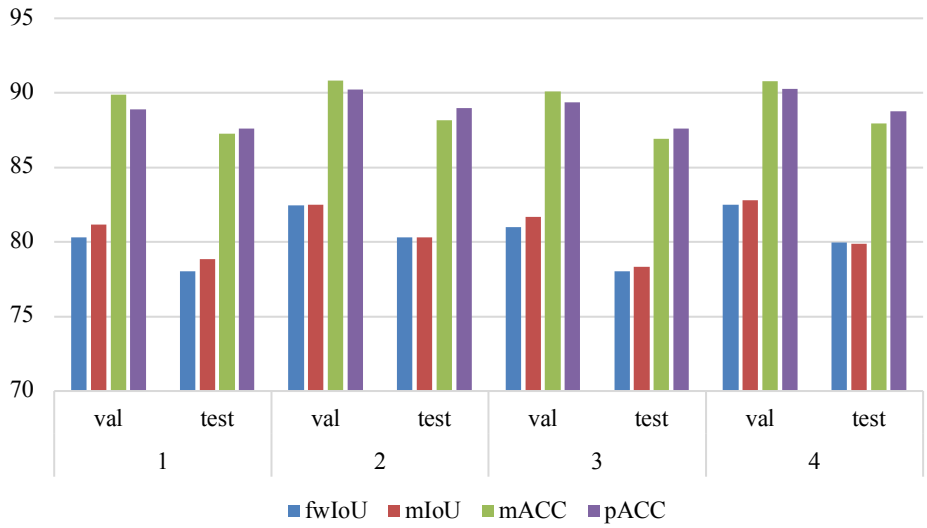

Figure 3.6 Evaluation metrics based on the validation and test datasets for the four models at 2,000 epochs.

Models 2 and 4 showed similar performances in four evaluation metrics based on the validation datasets. Both fwIoU and mIoU for Models 2 and 4 were about 82.5%, and mACC and pACC were about 90.8% and 90.2%, respectively, for both Models 2 and 4.

However, the performance of Model 2 on the test dataset was relatively better than that of Model 4 by about 1%. The test mACC and pACC of Model 2 were about 88.5% and test mIoU and fwIoU of Model 2 were about 80.3%. The test results of Model 2 were close to the validation results and also demonstrated that Model 2 had a decent prediction performance. Moreover, the training time of Models 2 and 4 were 1.19 and 1.85 hours for 2,000 epochs, respectively, which met the expectations because the backbone architecture of Model 4 had more layers. Accordingly, Model 2 was chosen for further analysis of surface drainage condition assessments because this model had a relatively better performance and shorter training time than Model 4.

Figure 3.7 shows the IoU (Intersection-over-Union) and ACC (accuracy) for each label on both the validation and test datasets predicted by Model 2. “No data” had the best performance among all labels, datasets, and evaluation metrics. This result was expected due to the clear boundary between different labels. By contrast, “Roadside channel” had the worst IoU among all labels for both datasets. Furthermore, this label had the smallest ratio of IoU to ACC for both datasets. By definition, the ratio of IoU to ACC represents the proportion of the area of ground truth to the area of the union of ground truth and prediction. Hence, “Roadside channel” had a relatively lower percentage of ground truth in the union of ground truth and prediction because it usually had a smaller area and unclear boundaries in an image than the other labels. However, the IoUs were still greater than 70%, demonstrating that Model 2 correctly and effectively identified roadside channels.

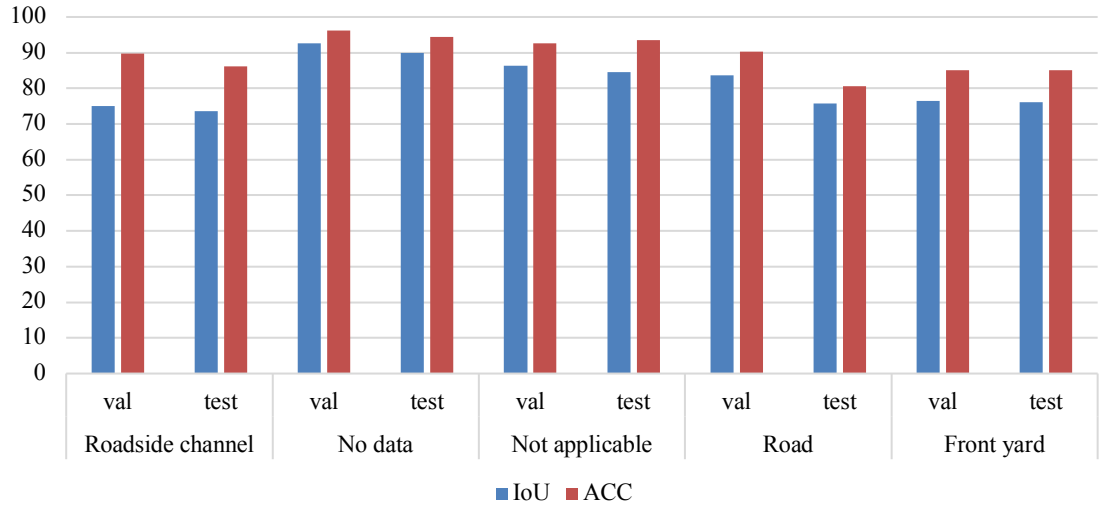

Figure 3.7 IoU and ACC for each label as predicted by Model 2.

Figure 3.8 presents a comparison between the ground truth and the prediction made by Model 2 for a test street block. Both numerical metrics and visualizations of the results of Model 2 demonstrated promising results in identifying different infrastructures and areas within a street block. Model 2 served as a benchmark for applying semantic segmentation to identify drainage infrastructures and adjacent land within a street block. Further studies are needed to improve the performance of the models in identifying infrastructures and adjacent land for this specific environment.

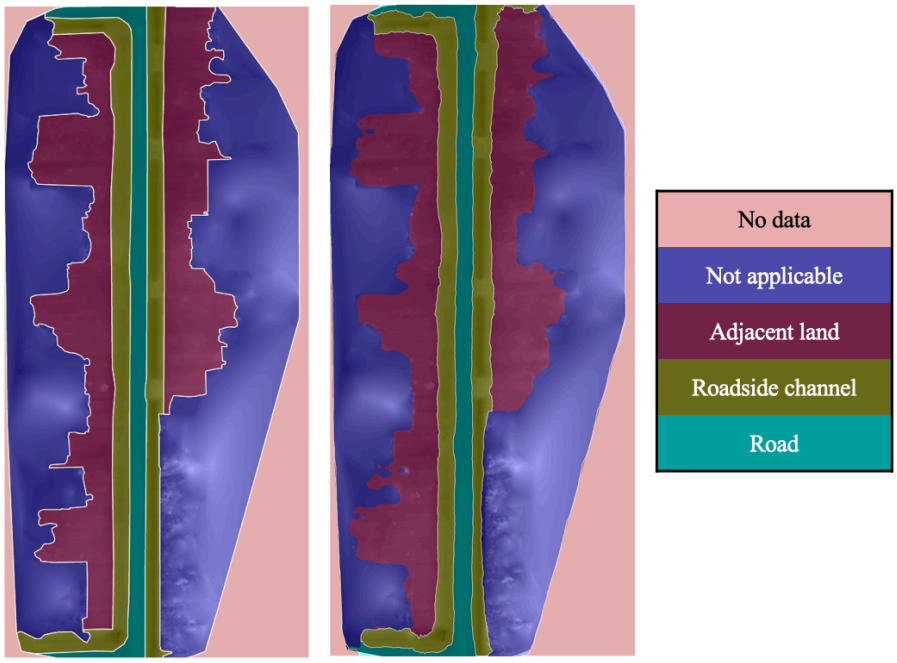

Figure 3.8 Comparison of ground truth and prediction of a test street block by applying Model 2.

3.6. Surface drainage condition evaluation

Surface drainage conditions were evaluated based on flow directions. The flow directions were calculated on the basis of DEMs within the area labeled as "Road", "Roadside channel", and "Adjacent land" of a street block by using TopoToolBox, a MATLAB toolbox (Schwanghart & Scherler, 2014). TopoToolBox requires that the calculated area cannot have any empty grid cell, but it has no limitation for the outer shape of the calculated area. Owing to this restriction, an additional data processing step was performed. The red circle in Figure 3.9 shows a small area labeled as "Not applicable" within an adjacent land area. Given that only the areas labeled as "Road", "Roadside channel", and "Adjacent land" (RRA) were determined, the small area labeled as "Not applicable" within RRF area became empty during calculation and caused errors. The blue

circle in Figure 3.9 represents the area labeled as “Adjacent land” but did not connect to the major portion of the area of “Adjacent land”. Thus, the additional data processing step considered the empty areas within the areas labeled as RRA. The small areas that did not connect to the major RRA area were removed.

The image was split into two groups: areas labeled as “No data” and “Not applicable” (NN) and areas labeled as RRA. Two conditions were then applied to this data processing step: (a) if the area of Group NN was not connected to figure boundaries, the area was treated as Group RRA, and (b) if the area of Group RRA was not connected to the largest portion of Group RRA, the area was treated as Group NN. Through this data processing step, Group RRA became a complete area without any empty grid cells. Before calculating flow directions, depressions in DEMs were needed to be cope with to obtain hydrologically correct results (Wang et al., 2019). Depressions shallower than four inches were filled, and other depressions were not changed to account for enclosed pits.

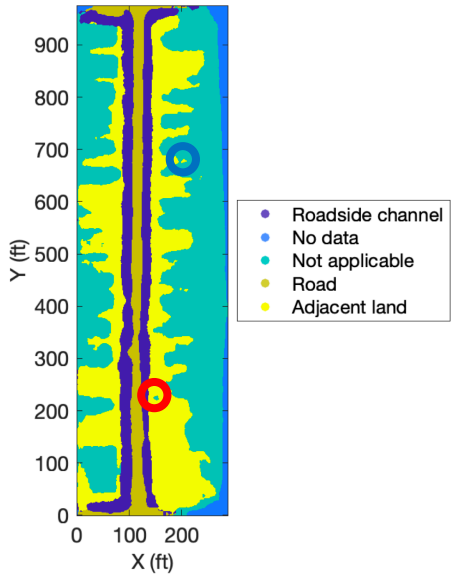

Figure 3.9 Example of unacceptable areas for TopoToolBox (marked in circles).

Flow directions were calculated by TopoToolBox as shown in the left of Figure 3.10. A darker shade indicates that more flows accumulated at a specific grid cell. The value of flow accumulation for a specific grid cell represents the number of upstream grid cells that are accumulated to that specific grid cell. It can be discovered that most of the flows were accumulated close to roadside channels. Cells were identified as parts of a flowline if the flow accumulation of the cell was greater than 14,400 cells, which was determined through trial and error to obtain the best possible identification results. It entails that a specific cell will collect water from at least 14,400 upstream cells. In other words, the cell will receive water that falls on areas at least 400 sq. ft in dimension because the grid size was set to 2 in × 2 in. The blue lines in the right side of Figure 3.10 shows the identified cells in which flow accumulation were greater than 14,400. The data were analyzed further to identify the end points of all major flowlines, or major end points, which indicate where water eventually drains. Given that 14,400 was a simple threshold, some of the cells along a major flowline fell within the threshold and caused the threshold to incorrectly identify the end points of flowlines as the actual end points (red arrow in Figure 3.10). Therefore, an additional data processing step was conducted to determine all major flowlines and their corresponding end points. The idea was that the end point of a flowline was not considered as the end point of a major flowline if it met the following conditions: (a) at least one starting point of the other flowlines was within 20 feet and (b) the flow accumulation at the end point of any of the corresponding flowlines was higher than the evaluated flowline. An example is shown in Figure 3.11. If any of the flow accumulation at the end points of three dashed lines was greater than the end points of the

evaluated flowline, the end point of the evaluated flowline was not considered as the end point of a major flowline. Otherwise, if the end point of the evaluated flowline had the largest flow accumulation compared with three dashed lines, the end point of the evaluated flowline was identified as an end point of a major flowline. Through this process, the major end points were identified (red crosses in Figure 3.12). The end points indicate the places where water would accumulate.

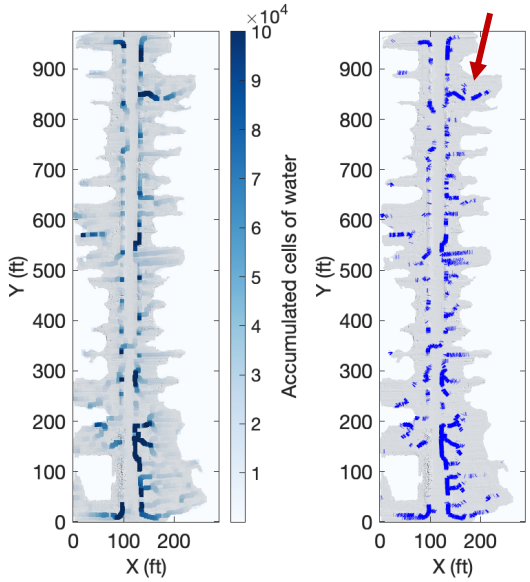

Figure 3.10 Flow directions calculated by TopoToolBox and the corresponding flowlines.

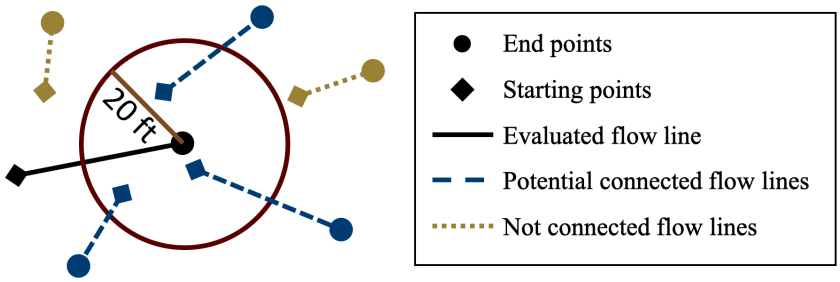

Figure 3.11 Schematic for recognizing the end points of major flowlines.

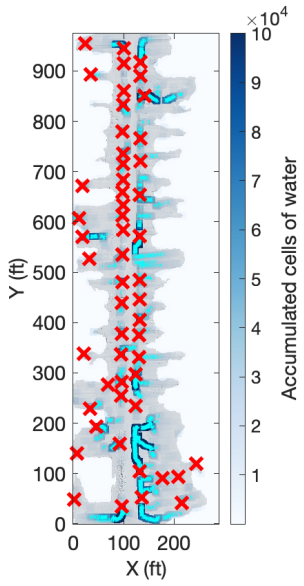

Figure 3.12 End points of the major flowlines within a street block.

3.7. Discussion

3.7.1. Discussion of drainage condition within a street block

The end points of major flowlines are critical for evaluating surface drainage conditions. In this study, we used a buffer of 10 feet from roadside channels identified by semantic segmentation to determine if a major end point was away from roadside channels. This parameter, off-channel major end points percentage (OMEP), indicating the percentage of major end points located away from drainage channels, is critical for evaluating surface drainage conditions. Figure 3.13 presents a visualization for comparing the major end points to roadside channels. In this street block, 25.5% (14 out of 55) of the major end points were at least 10 feet away from the roadside channels. These end points may lead to drainage issues. The nearest distances of each end point to roadside channels and their corresponding flow accumulation are shown in Figure 3.14. The flow

accumulation of the end points away from roadside channels were relatively lower than those in or close to roadside channels, except for points 5 and 11. For this street block, points 5 and 11 tended to accumulate more water than the other end points away from roadside channels. Hence these points require more attention to avoid ponding issues.

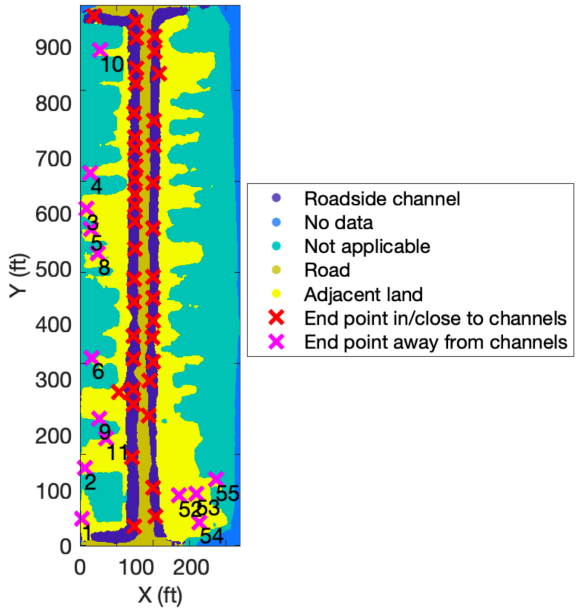

Figure 3.13 Visualization of the end points of major flowlines within a street block.

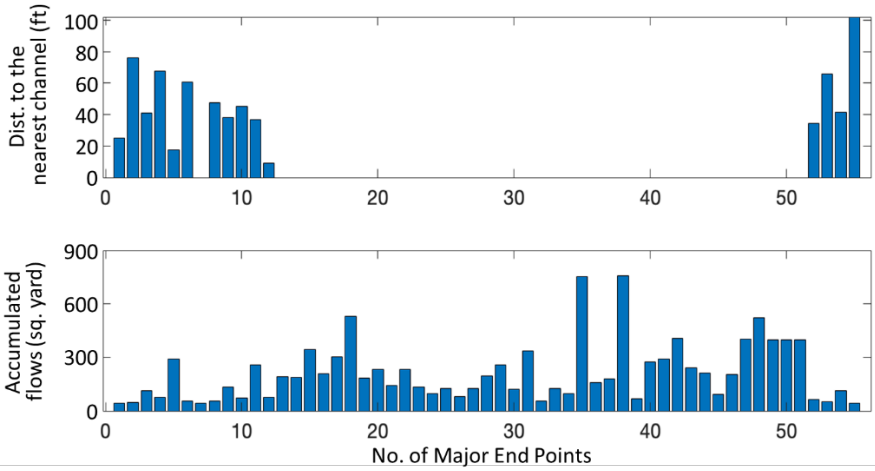

Figure 3.14 Distance to the nearest roadside channel and the corresponding flow accumulation.

3.7.2. Discussion of drainage condition among street blocks

The test dataset containing 10 street blocks was also evaluated following the aforementioned data processing steps. The results of the test dataset are shown in Table 3.2. Although the process for identifying the major end points was proposed and conducted, the end points identified may not be able to fully represent the actual end points because the summation of the flow accumulation area of the major end points within a street block may be higher or lower than the total evaluated areas of the street blocks as shown in Table 3.2. The flow accumulation area of all major end points of street block #8, for example, was greater than its total evaluated areas. Conversely, the flow accumulation area of all major end points of street block #3 was smaller than its total evaluated areas. These results were because of the calculation of flow directions. When the flow accumulation of a small pit was less than the threshold for identifying flowlines (i.e., 14,400), the end point in this pit was not identified as a part of a flowline and thus was not recognized as an end point of a major flowline. Contrariwise, when the flowline went through a relatively flat area, the flow spread to a certain length, converged at a point after the flat area, and started to accumulate again. Within this relatively flat area, the flow accumulation of a cell decreased along the flowline and even fell under the threshold for identifying flowlines. Once the length of this flat area was longer than 20 feet, a value was selected for recognizing major end points, the flow was treated as two separate major flowlines with their own end points. However, they actually belonged to one major flowline. The results shown in Table 3.2 was overestimated when this situation happened. Nevertheless, the flow accumulation of the major end points identified remained important

because they indeed indicated the amount of water that would be accumulated or diverged to a relatively flat area at a certain point. The average flow accumulation area per off-channel major end point (AFAA) are shown in Table 3.2. Street blocks #1, #2, and #9 had relatively high AFAA, indicating that a high water volume may not be conveyed to drainage channels appropriately. On the other hand, all major end points of street block #7 were in or close to roadside channels.

Table 3.2 Results of surface drainage condition evaluation for the test dataset.*

ID	FAA of all MEP**	Total evaluated area	FAA of all off-channel MEP	AFAA
1	15,951	18,692	4,108	164
2	15,385	20,775	3,259	163
3	11,961	16,292	1,464	105
4	14,068	17,019	2,642	106
5	12,299	14,266	1,061	152
6	10,757	14,375	1,183	118
7	8,320	9,334	-	-
8	20,613	14,584	516	103
9	16,756	13,176	1,770	161
10	24,456	15,862	687	86

*Unit: sq. yard
**FAA: flow accumulation area, MEP: major end points

The number of major end points and of major end points away from roadside channels can reflect the drainage condition of a street. As shown in Table 3.3, all major end points identified in street block #7 were in or close to roadside channels. Therefore, the surface drainage performed as expected. By contrast, about half of the major end points in street block #1 were away from roadside channels. These major end points may require additional inspections to prevent water ponding and flooding issues.

Table 3.3 Number of the major end points in each street block.

ID	Total No. of MEP*	No. of MEP away from roadside channels	OMEP (%)
1	53	25	47.2%
2	64	20	31.3%
3	55	14	25.5%
4	67	25	37.3%
5	50	7	14.0%
6	47	10	21.3%
7	23	0	0.0%
8	26	5	19.2%
9	41	11	26.8%
10	30	8	26.7%

*MEP: major end points

3.8. Summary, conclusions, and recommendations

Local topography affects the collection and convenience of storm runoff. Consequently, modeling local topography (e.g., neighborhood scale) is critical for generating realistic water-flow simulations and evaluating the effectiveness of drainage systems. This study provides a method for surface drainage condition assessment that incorporates semantic segmentation (a computer vision technique) and flow direction determination. Fifty lidar images representing 50 street blocks in Houston, Texas were used and split into 30, 10, and 10 images for training, validation, and test datasets, respectively. Four semantic segmentation models with different combinations of ResNet architectures and augmentation methods were trained on the basis of an Imagenet-1k pretrained model. The results show that all four models have the ability to identify key drainage and land features within a street block; however, one model was selected for its relatively superior performance. The selected model has intersection-over-union (IoU) and accuracy (ACC) values of about 80.3% and 88.5% for the test dataset, respectively.

Flow direction was determined in the areas labeled as “Road”, “Roadside channel”, and “Adjacent land” for each street block. An additional data processing step was conducted to identify the end points of all major flows that have higher flow accumulation in nearby areas. Surface drainage condition was evaluated by determining the closeness of a major end point to roadside channels. Ten feet was used as a threshold to determine if a major end point was close to or away from a roadside channel. The results of the test dataset showed that street block #7 had no major end point away from roadside channels. By comparison, about half of major end points in street block #1 were away from roadside channels. Moreover, street block #1 had the highest average flow accumulation of major points away from roadside channels. Therefore, among the test datasets, street block #1 may need additional maintenance to avoid water ponding and address potential localized flooding.

The presented method can be beneficial for both public works agencies and local residents by providing drainage condition information at the neighborhood and street levels. Using this information, proactive improvements can be implemented before the start of pluvial seasons to mitigate the damages caused by flooding and water ponding. Finally, further studies are needed in three areas: (a) improve the segmentation algorithms to enhance their performance in identifying drainage infrastructure and adjacent land areas within a street block, (b) integrate the presented method with hydrology techniques to simulate water flow more precisely, and (c) integrate roadside channel condition information (e.g., blockages, erosion, etc.) to obtain a more comprehensive assessment of drainage conditions.

4. ASSESSMENT OF DRAINAGE CONDITIONS IN RESIDENTIAL AREAS WITH ROADSIDE CHANNEL SYSTEMS: CASE STUDIES

4.1. Introduction

Assessing drainage conditions to ensure drainage capabilities at the neighborhood level can help public works agencies to develop maintenance plans and mitigation strategies to guard against pluvial floods. Similarly, these assessments can inform residents about problem drainage areas and possible solution. Current drainage condition assessment methods have two common shortcomings: (a) they depend on manual visual inspection, which is a time-consuming and labor-intensive process, and (b) they ignore areas outside the street right-of-way (e.g., adjacent front yards), despite the interdependency between public drainage system (e.g., roadside channel) and adjacent private properties. The objective of this study is to assess the drainage conditions in two Texas communities that are socially and physically vulnerable to flooding and stormwater-related hazards using automated methods. Recently developed automated inspection methods (Lee & Gharaibeh, 2020, 2021) that use data from mobile lidar (light detection and ranging) have been used for assessing the drainage conditions in two case studies: Sunnyside (a neighborhood within the City of Houston) and Rockport (a neighborhood adjacent to the City of Rockport.

The remainder of this paper is organized as follows: In the next section, an overview of the literature and practices on the assessment of drainage systems in residential areas are provided. The following sections introduce the evaluation methods used in this study and the details about the two study communities. Results and Discussion

section shows the results obtained from applying the evaluation methods and demonstrates the discussion and comparison between the study communities. Finally, the research summary and conclusions are presented.

4.2. Review of drainage condition assessment literature and practices

4.2.1. Assessment of drainage systems in residential areas

Systematic inspection and evaluation of drainage infrastructure aids both public works agencies and property owners in identifying problem areas and planning the allocation of financial resources to address these problems in the most cost-effective manner (Frank & Falconer, 1990; Molzahn & Burke, 1986). Manual inspection methods with random sampling are usually used for drainage system assessments in residential areas. However, manual inspection methods can be time consuming and subjective, especially for quantitative measurements (Lee & Gharaibeh, 2020). To address the challenge of evaluating drainage systems in local communities, Oti et al. (2019) developed citizen science methods for collecting condition data. Although volunteer citizen scientists can provide timely and high-quality data related to the conditions of drainage systems, they tend to have difficulties obtaining detailed quantitative measurements. Lidar technology offers opportunities to collect infrastructure data with high density and quality. For example, G. Cha et al. (2019) used terrestrial lidar to construct a building information model for the detection of the shape deformation of bridge structures. Mobile lidar, in particular, has been used most recently for assessing the conditions of roadway drainage and pavements (Chou et al., 2017; Gurganus et al., 2017; Oliveira & Correia, 2009). For example, Gurganus et al. (2017) determined the drainage ability of highways by using

mobile lidar to produce a preliminary drainage design. However, methods for the assessment of drainage systems in residential areas remain limited in the literature. Lee and Gharaibeh (Lee & Gharaibeh, 2020, 2021) developed an automated method for evaluating the drainage conditions of roadside channels and adjacent land using mobile lidar; the methods was found to be reliable in obtaining information on drainage conditions within street blocks.

4.2.2. Design guidelines for drainage channels

This work reviewed the design guidelines for channels and driveways in multiple states across the entire US. Grass-lined open channels are widely used in residential areas and are included in most design manuals. These channels can be natural or constructed channels that are graded to as-designed dimensions and established with suitable vegetation for a stable and safe conveyance of runoff. According to the reviewed guidelines, several design criteria should be met for drainage channels. These criteria include capacity, velocity, vegetation, roughness, and geometric attributes. Blockage tends to occur in pipes or culverts placed beneath driveways, which connect homes or buildings to streets. Therefore, the criteria for the width of driveways (which matches the length of the subsurface pipe or culvert) were also reviewed in this study. This review focuses on the design criteria for geometric dimensions, as these criteria are most relevant to the drainage condition assessment methodology used in the case studies.

Table 4.1 provides a summary of geometric design criteria for channels and driveways in 22 different cities, counties, and states in the US. Generally, these criteria are set to meet drainage (water flow, pollution, erosion, etc.) as well as safety performance requirements. However, this paper is concerned with the drainage aspects only. The requirement for channel minimum depth varies from 1 ft to 2 ft. In some cases, minimum required channel depth is not specified directly; instead, it is calculated on the basis of peak flow and the required minimum channel freeboard, which ranges from 6 in to 2 ft. The required minimum channel bottom width ranges from 2 ft to 4 ft. However, most agencies adopt 2 ft as the criterion for channel bottom width. For the side slope, the variation among the reviewed guidelines is relatively small. The requirements for the foreside and backside slope are generally the same, and they range from 1V:2H to 1V:4H. Some design manuals, however, use different requirements for foreside and backside slopes. For example, King County in Washington State uses 1V:3H for the foreside slope and 1V:2H for the backside slope. The required minimum longitudinal slope ranges from 0.1% to 1%. The requirement for driveway maximum width, or the length of subsurface pipes or culverts, varies greatly, ranging from 20 ft to 40 ft. The review herein shows that the guidelines published by different government agencies vary greatly to meet the needs of local environments. As shown in a previous study (Lee & Gharaibeh, 2020), these criteria can serve as references for evaluating the performance of drainage channels by using mobile lidar.

Table 4.1 Summary of roadside drainage geometric criteria required by different public work agencies.

City/County/State	Depth	Bottom width	Side slope (V/H)	Longitudinal slope (%)	Driveway width	Freeboard
Harris County, TX[2]	1.5 ft-4 ft	> 2 ft	< 1/2-1/3	> 0.1	< 36 ft	NA
Aransas County, TX[3]	NA	NA	< 1/4	NA	< 24 ft	> 1 ft
Houston City, TX[4]	< 4 ft	> 2 ft	< 1/3	> 0.1	NA	NA
Galveston County, TX[5]	1.5 ft-4 ft	> 2 ft	< 1/2-1/3	> 0.1	NA	NA
Cook County, IL[6]	> 3 ft	> 2 ft	< 1/3	> 0.3	NA	> 1 ft
King County, WA[7]	NA	> 2 ft	< 1/2-1/3	> 0.5	< 30 ft	NA
San Diego County, CA[8]	1ft-5 ft	NA	< 1/3	> 0.5	NA	> 0.5 ft
Lincoln City, NE[9]	NA	NA	< 1/4	< 1	NA	> 1ft
Jefferson County, CO[10]	< 5 ft	> 4 ft	< 1/4	NA	< 24 ft	> 1 ft
Douglas County, CO[11]	< 5 ft	NA	< 1/4	< 0.6	< 22 ft	> 2 ft
District of Columbia[12]	NA	4 ft-8 ft	< 1/3	< 2	< 25 ft	> 1 ft
Georgia State[13]	NA	2 ft-6 ft	< 1/3	1-2	< 20 ft	NA

[2] (Arthur L. Storey, 1988; Arthur L. Storey & Freeman, 2005)
[3] (Aransas County, 2012)
[4] (Haddock & Myers, 2018)
[5] (Badger, 2013)
[6] (Cook County, 2012, 2020)
[7] (Brater, 2016)
[8] (San Diego County, 2005)
[9] (Lincoln County, 2000)
[10] (Jefferson County Planning and Zoning Division, 2019)
[11] (Douglas County, 2008, 2015)
[12] (Hoffmann et al., 2012; Tregoning & Bellamy, 2019)
[13] (Haubner et al., 2001; State of Georgia Department of Transportation, 2019)

Honolulu City and County, HI[14]	> 1.5 ft	2 ft-8 ft	< 1/3	< 2	< 20 ft	NA
Marion County, OR[15]	> 1 ft	> 2 ft	< 1/3	> 0.5	< 24ft	> 0.5 ft
Fort Wayne City, IN[16]	NA	NA	< 1/3	> 0.5	NA	> 2 ft
Clark County, NV[17]	1ft-5 ft	> 5 ft	< 1/3	> 0.4	NA	> 1 ft
Hillsborough County, FL[18]	2 ft-3.5 ft	> 3 ft	< 1/4	> 0.1	NA	NA
Fairfax City, VA[19]	NA	> 3 ft	<1/3	NA	NA	NA
New York State[20]	NA	2 ft-8 ft	< 1/2-1/3	< 4	< 24 ft	> 0.5 ft
Charlotte City, NC[21]	NA	NA	< 1/2	NA	< 20 ft	> 0.5 ft
Tulsa City, OK[22]	NA	NA	< 1/4	< 1	< 20 ft	> 1 ft
Rhode Island State[23]	NA	2 ft-8 ft	< 1/2	1-2	NA	NA

4.3. Drainage system evaluation method

In this study, the drainage system is evaluated based on the geometric attributes of the roadside channels and two additional parameters that describe the off-channel drainage conditions. The geometric attributes were adopted from an automated method for

[14] (City and County of Honolulu Department of Planning and Permitting, 2000; Tanoue, 2011)
[15] (Marion County Public Works, 1990, 2012)
[16] (Fort Wayne City, 2017)
[17] (Clark County, 1999)
[18] (Hillsborough County, 2015)
[19] (City of Fairfax, 2017)
[20] (New York State, 2001, 2008)
[21] (City of Charlotte, 2013, 2014)
[22] (City of Tulsa, 2017; Oklahoma Department of Transportation, 1992)
[23] (Rhode Island State, 2010)

evaluating roadside drainage channels in urban residential areas proposed by Lee and Gharaibeh (2020). Two parameters were used to assess off-channel drainage conditions: (a) percentage of major end points (MEP) located away from drainage channels, and (b) average cumulative flow area away from drainage channels. Specifically, the evaluation criteria are based on the following parameters:

- Channel geometric attributes
    - Channel depth
    - Channel bottom width
    - Channel side slope
    - Channel longitudinal slope
    - Subsurface pipe/culvert length
    - Subsurface pipe/culvert density
- Off-channel drainage attributes
    - Off-channel major endpoints percentage (OMEP): Percentage of major endpoints located away from drainage channels.
    - Average flow accumulation area per off-channel major endpoint (AFAA)

These parameters provide a fairly comprehensive understanding of drainage conditions within and across street blocks. The drainage conditions of street blocks and neighborhoods can be evaluated to ensure that water is collected effectively by the drainage system and conveyed to the design discharge points. This study implemented these criteria to two local communities in Texas to demonstrate its use for assessing drainage conditions in residential areas.

In this study, the raw data were obtained from a single laser mobile lidar system. The geometric parameters were determined by analyzing the lidar raw data using statistical and heuristic methods (Lee & Gharaibeh, 2020). OMEP and AFAA values were determined using computer vision and flow direction techniques (Kirillov et al., 2019; Lee & Gharaibeh, 2021; Tarboton, 1997).

4.4. Study sites

The drainage conditions of roadside channels and adjacent land were evaluated for two Texas communities with relatively high vulnerability to flooding and drainage-related hazards. These communities are located in Harris County (Sunnyside community) and Aransas County (Rockport community) as shown in Figure 4.1. The Sunnyside community is older than the Rockport community (the median year structure built, a proxy for community age, is 1964 for Sunnyside and 1980 for Rockport). We chose these study areas because these communities suffer from localized flooding and utilize roadside channels as their primary stormwater drainage systems for runoff control. A summary of the characteristics of these two communities is provided in Table 4.2 and discussed in the following sections.

Figure 4.1 Sites of case studies (Harris and Aransas Counties in Texas).

Table 4.2 Characteristics of the case study communities.

	Sunnyside	Rockport
Location	Southern part of Harris County, Within the city of Houston	Center of Aransas County, Adjacent to the city of Rockport
Population density[24]	5.84 (per acre)	0.65 (per acre)
% of developed lands (Impervious surfaces)[25]	100 % developed lands - 49.10 % medium-intensity - 41.34 % low-intensity - 5.17 % high-intensity - 4.39 % open space	96.49 % developed lands - 53.67 % low-intensity - 29.39 % open space - 11.82 % medium-intensity - 1.60 % high-intensity 3.51% undeveloped lands
Race/ethnicity[24]	82.00% non-Hispanic black 14.84% Hispanic 3.16% non-Hispanic white	70.94% non-Hispanic white 27.69% Hispanic 1.37% non-Hispanic black

[24] ("U.S. Census – 2018 ACS (American Community Survey) 5-year Estimates," 2019)
[25] ("MRLC (Multi-Resolution Land Characteristic Consortium) – NLCD (National Land Cover Database) 2016 Land Cover (CONUS)," 2019)

Median household income[26]	$ 26,845	$ 39,091
% of households below the poverty level[26]	26.04 %	10.52 %
Median year structure built[26]	1964	1980
Social vulnerability index[27]	0.9121	0.6062
Major flooding[28]	Localized and riverine flooding	Localized and coastal flooding
Floodplain[28]	Outside of the floodplain	Outside of the floodplain
Ponding / Inundation[28]	Shallow ponding of 0.5 to 2 ft depth in some parts of the community	2 ft of ponding depth in the north-west part of the community

4.4.1. Sunnyside community

The Sunnyside neighborhood is located in the southern part of Harris County within the city of Houston (Figure 4.2). The population density in this community is 5.84 (per acre), with 1,328 of the total population occupying 227.5 acres ("U.S. Census – 2018 ACS (American Community Survey) 5-year Estimates," 2019). All the community areas are developed lands, including 49.10% medium-intensity development, 41.34% low-intensity development, and 5.17% high-intensity development areas, as well as 4.39% open space areas ("MRLC (Multi-Resolution Land Characteristic Consortium) – NLCD

[26] ("U.S. Census – 2014-2018 ACS (American Community Survey) 5-year Data Profile," 2019; "U.S. Census – 2018 ACS (American Community Survey) 5-year Estimates," 2019)
[27] (Agency for Toxic Substances and Disease Registry, 2020; Flanagan et al., 2011)
[28] (Aransas County, 2011, 2017a, 2017b; City of Houston, 2018; "GIMS – GIM Public," 2020; "Harris County Flood Control Districts – Flood Education Mapping Tool," 2020; Rice University's Baker Institute for Public Policy, 2019)

(National Land Cover Database) 2016 Land Cover (CONUS)," 2019). The Centers for Disease Control and Prevention (CDC) Social Vulnerability Index (SVI) of this community is 0.9121, which indicates high social vulnerability relative to Texas (Agency for Toxic Substances and Disease Registry, 2020). SVI indicates the relative vulnerability of every US Census tract (subdivisions of counties for which the Census collects statistical data) (Agency for Toxic Substances and Disease Registry, 2020). SVI ranks the tracts based on percentiles of 15 social factors, including poverty, lack of access to transportation, crowded housing, unemployment, minority status, and disability. Percentile ranking values range from 0 to 1, with higher values indicating greater social vulnerability (Agency for Toxic Substances and Disease Registry, 2020). The social factors included in the SVI may weaken a community's ability to prevent human suffering and financial loss in a disaster (Agency for Toxic Substances and Disease Registry, 2020).

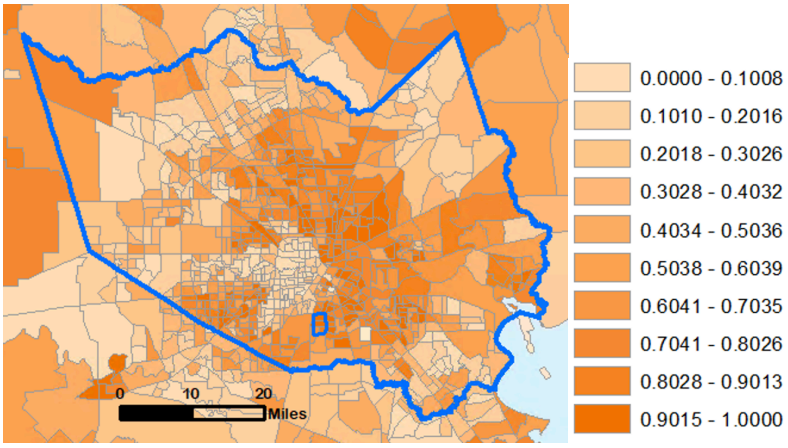

Figure 4.2 Location and CDC SVI of the Sunnyside community (Harris County, TX).

Harris County is vulnerable to localized and riverine flooding due to frequent excessive rainfall events and rapid urban growth (City of Houston, 2018). Recent heavy

rainfall events (e.g., flash flood in June 2006, Memorial Day flood in May 2015, Tax Day flood in May 2016, and Hurricane Harvey in August 2017) caused devastating flood damages in Harris County (City of Houston, 2018). Although the Sunnyside community is located outside the floodplain, it sits adjacent to a 100-year floodplain. This community suffers from localized flooding and poor drainage; shallow ponding with a depth of 0.5-2 ft in some parts of the community was recorded during past rainfall events ("GIMS – GIM Public," 2020; "Harris County Flood Control Districts – Flood Education Mapping Tool," 2020; Rice University's Baker Institute for Public Policy, 2019). During hurricane Harvey, this community experienced high flood damage. Around 64% of housing units were affected and thus received assistance from federal emergency management agency (FEMA) ("FEMA – OpenFEMA Dataset: Individual Assistance Housing Registrants Large Disasters – V1," 2019).

4.4.2. Rockport community

This community is located in the center of Aransas County, which is adjacent to the city of Rockport, as shown in Figure 4.3. The population density in this community is 0.65 (per acre), with 1,163 of the total population occupying 1,785.5 acres ("U.S. Census – 2018 ACS (American Community Survey) 5-year Estimates," 2019). Most of the community areas are developed lands (96.49%), including 53.67% low-intensity development, 29.39% open space, 11.82% medium-intensity development, and 1.60% high-intensity development areas ("MRLC (Multi-Resolution Land Characteristic Consortium) – NLCD (National Land Cover Database) 2016 Land Cover (CONUS)," 2019). The remaining areas are undeveloped lands with forest and herbaceous land cover

("MRLC (Multi-Resolution Land Characteristic Consortium) – NLCD (National Land Cover Database) 2016 Land Cover (CONUS)," 2019). The CDC SVI of this community is 0.6062, which indicates moderate social vulnerability relative to Texas (Agency for Toxic Substances and Disease Registry, 2020).

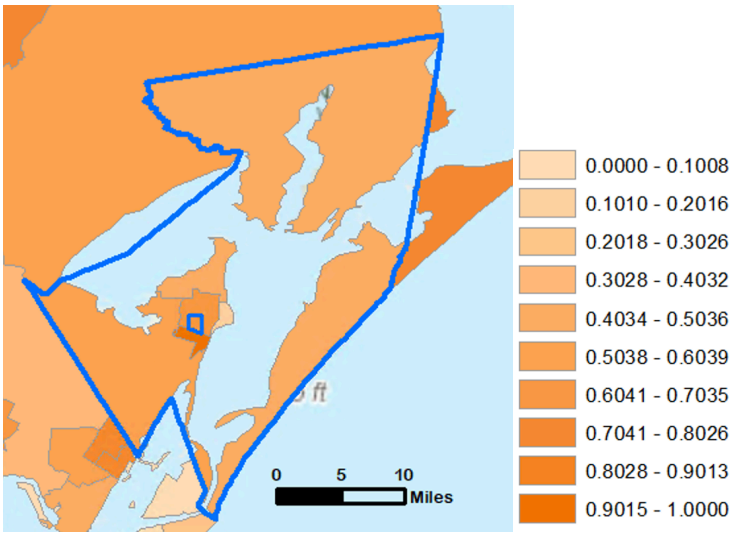

Figure 4.3 Location and CDC SVI of the Rockport community (Aransas County, TX).

Aransas County, as a coastal county, is susceptible to coastal and localized flooding (Aransas County, 2017b). Recent heavy rainfall events (e.g., flash flood in July 2006, flash flood in June 2015, Hurricane Harvey in August 2017, and south Texas heavy rainfall in September 2018) caused flood damages in Aransas County (Aransas County, 2017b; "NOAA – South Texas Heavy Rainfall - September 2-16, 2018," 2020). The community is located outside the floodplain, but it continues to suffer from frequent localized flooding (Aransas County, 2017a, 2017b). Specifically, the northwest part of the community recorded 2 ft of ponding depth during past rainfall events (Aransas County, 2011). During hurricane Harvey, 34.59% of housing units in this community suffered from

wind and flood damage and thus received FEMA assistance ("FEMA – OpenFEMA Dataset: Individual Assistance Housing Registrants Large Disasters – V1," 2019).

4.5. Results and discussion

This section presents the results of the drainage condition evaluation for the two studied communities and provides a statistical comparative analysis of these results. The Sunnyside case study consists of 10 street blocks with a total length of 1.67 centerline miles. The Rockport case study consists of 20 street blocks with a total length of 3.02 centerline miles.

4.5.1. Results and discussion for the Sunnyside community

The pass/fail evaluation results for the Sunnyside community based on the requirements published by Harris County are shown in Table 4.3. In this community, no street block completely meets the requirement published by Harris County. Among the six attributes, all the street blocks meet the average P/C length requirement and only one channel does not meet the requirement for channel bottom width. However, the side and longitudinal slopes are the predominant types of failure in this community. More than half of the channels are not in compliant with the side slope and longitudinal slope requirements in this community, suggesting that these issues require greater attention to ensure that the channels in this community can convey stormwater as designed.

Table 4.3 Pass/fail drainage evaluation results for the Sunnyside community.

Street Block		Channel Depth	Bottom Width	Left Side Slope	Right Side Slope	Avg. P/C Length	Longitudinal Slope	P/C Density
1	L	P	P	F	F	P	F	38.63%
	R	P	P	F	P	P	P	39.09%
2	L	P	P	P	P	P	P	17.56%
	R	F	P	P	P	P	P	27.93%
3-1	L	P	F	F	P	P	F	25.44%

3-2	R	P	P	P	P	P	F	22.06%
	L	P	P	P	P	P	F	17.52%
4-1	R	P	P	P	P	P	P	16.08%
	L	P	P	P	P	P	P	22.75%
4-2	R	P	P	F	F	P	P	28.09%
	L	P	P	P	F	P	P	13.47%
5-1	R	P	P	P	P	P	P	15.40%
	L	F	P	P	P	P	P	28.70%
5-2	R	F	P	F	P	P	F	22.68%
	L	P	P	P	P	P	P	15.08%
6-1	R	F	P	P	P	P	P	16.95%
	L	P	P	F	F	P	P	22.82%
6-2	R	P	P	F	P	P	F	18.17%
	L	P	P	P	F	P	P	17.40%
	R	P	P	P	P	P	P	15.57%

Furthermore, the direction of the longitudinal slope is also critical to ensure that the channel can drain water to the correct discharge points or downstream rivers. Figure 4.4 demonstrates the directions of the longitudinal slopes in the Sunnyside community. The dotted arrows indicate that the longitudinal slope is less than 0.1% (i.e., too flat according to the requirement published by Harris County). According to the Public Utility Map published by the City of Houston ("GIMS – Public Utility Map," 2020), the design discharge points for this community are all located at the end of block #1. Figure 4.4 shows that most of the channels have longitudinal slope directed toward block #1, except the right channels of street #3 and street block #6-1. Therefore, this evaluation indicates that street #3 channels need improvement to correct their longitudinal slopes and drainage directions.

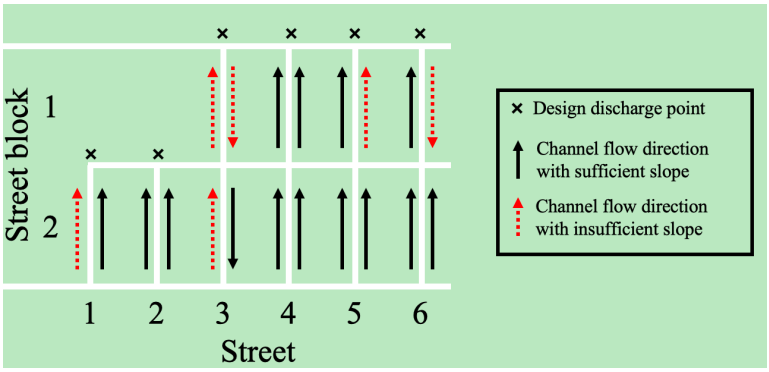

Figure 4.4 Directions of longitudinal slopes for roadside channels in the Sunnyside community.

The results of the evaluations of the off-channel drainage conditions in the Sunnyside community are shown in Table 4.4. For OMEP, four out of the 10 street blocks have OMEP higher than 30%, which indicates that 30% of the major end points are located away from the roadside channels. The combination of OMEP and relatively high AFAA indicates that those major end points may accumulate stormwater and thus could become potential areas for standing water. For example, Street block #3-1 has the second highest AFAA, but it has the lowest OMEP of street block. This combination indicates that Street block # 3-1 has a few low point areas, but these areas are likely to accumulate large amount of water due to their relatively high AFAA. On the other hand, street block #2 has the second-lowest OMEP and AFAA. This combination indicates that street block #2 has relatively low potential to suffer from ponding issues because most of the major end points are located in the drainage system and the flow accumulation away from the drainage system is relatively low.

Table 4.4 Results of evaluations of off-channel drainage conditions for the Sunnyside community.

Street block	MEP away from roadside channels/areas	Total MEP	OMEP	AFAA (sq. yard)
1	9	32	28.13%	93
2	6	31	19.35%	93
3-1	7	50	14.00%	152
3-2	25	67	37.31%	106
4-1	27	66	40.91%	130
4-2	23	76	30.26%	145
5-1	10	47	21.28%	118
5-2	18	67	26.87%	168
6-1	14	55	25.45%	105
6-2	17	54	31.48%	147

Overall, street block #3-1 has the most concerning drainage condition considering both on- and off-channel conditions. This block received two fails on the longitudinal slopes of roadside channels, has the second-highest AFAA, and has incorrect longitudinal slope direction in the right channel. Thus, corrective actions may be necessary by both property owners (to address potential off-channel ponding issues) and the municipal authorities (to address channel slope issues).

4.5.2. Results and discussion for the Rockport community

Rockport community consists of four streets, two of which have roadside channels. The other two streets lack any built drainage systems and thus drain water in an ad hoc manner using unimproved areas adjacent to the streets. Therefore, only the two streets with open channels were evaluated using the six channel condition attributes; the other two streets without open channels were evaluated in terms of the off-channel drainage conditions and longitudinal slopes of the adjacent land only. As Aransas County does not

have requirements for every attribute evaluated in this study, the pass and fail results of channel depth, channel bottom width, and longitudinal slope in Table 4.5 were based on the requirements published by Harris County. Table 4.5 shows the evaluation results for the two streets that have roadside channel in the Rockport community.

Table 4.5 Pass/fail drainage evaluation results for the Rockport community.

Street Block		Channel Depth	Bottom Width	Left Side Slope	Right Side Slope	Avg. P/C Length	Longitudinal Slope	P/C Density
7-1	L	P	P	P	P	P	F	13.54%
	R	P	P	P	F	P	F	11.66%
7-2	L	P	P	P	P	P	F	14.89%
	R	P	P	P	F	P	F	8.86%
7-3	L	P	P	P	P	P	P	15.09%
	R	P	P	P	F	P	P	8.06%
7-4	L	P	P	P	P	P	P	25.21%
	R	F	P	P	P	P	P	20.45%
7-5	L	F	P	P	P	P	F	21.38%
	R	F	P	P	F	P	F	18.92%
10-1	L	P	P	F	P	P	P	10.44%
	R	F	P	P	P	P	P	13.36%
10-2	L	P	P	F	P	P	F	24.87%
	R	F	P	P	P	P	F	16.85%
10-3	L	P	P	P	P	P	F	18.69%
	R	P	P	P	P	P	F	9.80%
10-4	L	P	P	F	P	P	P	14.49%
	R	P	P	P	F	P	P	25.08%
10-5	L	-	-	-	-	-	P	-
	R	F	P	P	F	P	F	9.69%

In this community, all channel bottom widths and average lengths of pipes and culverts meet the requirements; most of the side slopes also do. The average channel bottom width is 5.51 ft, which is more than two times the minimum requirement. However, more than half of the street blocks fail with regard to the channel depth and longitudinal slope. All street blocks, except street blocks #7-3 and #10-4, have at least a fail for either

the channel depth or the longitudinal slope. Hence, channel depth and longitudinal slope are the primary concerns.

Figure 4.5 shows the directions of the longitudinal slopes for the Rockport community. The dotted arrows show the longitudinal slopes that are less than 0.1%. The roadside slope directions indicate that most of the water in this community is conveyed to both ends of the streets, which are blocks #1 and #5. However, street blocks #7-3 and #7-4 meet at a low point (i.e., form a concave up vertical curve). A similar problem occurs at the right channel of street blocks #8-3 and #8-4, and the left channel of street blocks #10-4 and #10-5. This problem is more pronounced in street blocks #7-3 and #7-4 and the left channel of street blocks #10-4 and #10-5 because they have longitudinal slopes that are greater than 0.1%. These values thus raise concerns about these areas possibly accumulating water instead of carrying water to the discharge points. Generally, grade adjustments or channel maintenance may be needed to address these problems.

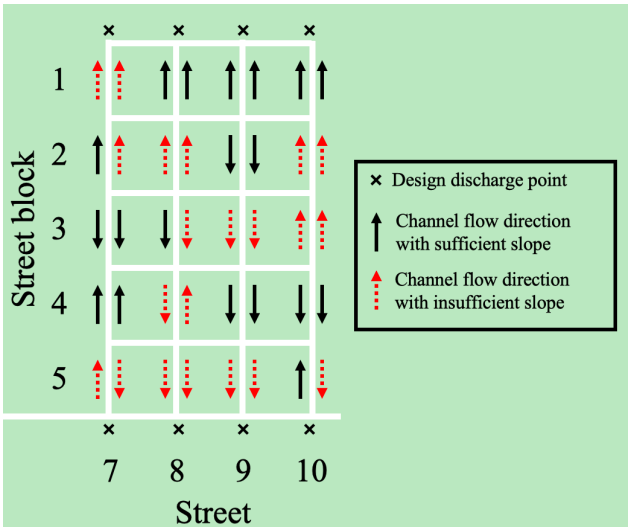

Figure 4.5 Directions of longitudinal slopes for Rockport community.

The results of the evaluations of the off-channel drainage conditions in the Rockport community are shown in Table 4.6. All four streets in the Rockport community were evaluated for their off-channel drainage conditions, including the two streets that do not have open drainage channels (i.e., streets #8 and #9). Among all street blocks, only three street blocks have OMEP higher than 30%, and all of them are in the same street, that is, street #7. Street blocks #7-2, #7-3, and #7-4 have the highest OMEP among the study area and have relatively higher AFAA than those of the other street blocks in this community. This combination indicates that Street blocks #7-2, #7-3, and #7-4 suffer from the worst scenario, which consists of multiple low point areas with high accumulation of water due to high AFAA. Consequently, these street blocks are susceptible to water ponding problems. Street block #8-4, on the other hand, appears to be the least susceptible to off-channel ponding issues as indicated by its low OMEP and AFAA values.

Table 4.6 Results of evaluations of off-channel drainage conditions for the Rockport community.

Street block	MEP away from roadside channels/areas	Total MEP	OMEP	AFAA (sq. yard)
7-1	8	41	19.51%	100
7-2	16	43	37.21%	155
7-3	13	40	32.50%	152
7-4	15	43	34.88%	220
7-5	10	45	22.22%	89
8-1	8	30	26.67%	86
8-2	6	30	20.00%	87
8-3	5	26	19.23%	103
8-4	3	37	8.11%	107
8-5	7	29	24.14%	125
9-1	6	27	22.22%	107
9-2	2	19	10.53%	103
9-3	4	28	14.29%	303

9-4	6	34	17.65%	116
9-5	8	35	22.86%	228
10-1	8	48	16.67%	97
10-2	8	38	21.05%	119
10-3	11	44	25.00%	119
10-4	8	33	24.24%	86
10-5	11	41	26.83%	161

In the Rockport community, most of the channels have at least one issue regarding the channel depth or longitudinal slope. Overall, street blocks #7-2, #7-3, and #7-4 have the most concerning drainage condition considering both on- and off-channel conditions. These street blocks suffer from concave up issues in the longitudinal direction and have relatively high OMEP and high AFAA. Thus, corrective actions may be necessary by both property owners (to address potential off-channel ponding issues) and the municipal authorities (to address channel longitudinal slope issues).

4.5.3. Discussion and comparative analysis of studied communities

To compare the drainage conditions in the two communities objectively, two comparisons are made: (a) percentage of channels passing the minimum requirements (i.e., passing rate), and (b) the magnitude of the physical measurement (statistical analysis of measurement values).

Table 4.7 compares the passing rates for roadside channels in the two communities. It can be seen that there is no significant difference between the passing rates except for the longitudinal slope. As discussed earlier, Aransas County does not have requirements for channel depth, channel bottom width, and longitudinal slope; thus, the passing requirements for these attributes were based on the requirements published by Harris

County. Almost half of the fails in the Rockport community are due to longitudinal slopes. By contrast, the fails in the Sunnyside community are distributed across the evaluation attributes.

Table 4.7 Channel geometric attributes passing rates for the two studied communities.

Channel Attributes	Sunnyside		Rockport		Proportion test P-value
	n	Passing rates	n	Passing rates	
Channel Depth	20	80%	19	68%	0.408
Bottom Width	20	95%	19	100%	-
Side Slope	40	70%	38	76%	0.530
Avg. P/C Length	20	100%	19	100%	-
Longitudinal Slope	20	70%	19	42%	0.079
All	120	81%	114	77%	0.494

To understand the differences between the two communities in terms of the physical measurements, a Kruskal-Wallis one-way analysis of variance (ANOVA) was performed on the channel attributes (Table 4.8). In addition to the channel geometric attributes, the cross-sectional area and channel capacity, or flow rate, were also calculated and compared. Manning's Equation (Manning, 1891), was used for estimating channel capacity (equation (4-1), one of the most commonly used equations for open channel flow. It considers flow cross-sectional area and longitudinal slope and is used for uniform flow in open channels as a basis for channel design. For comparison purposes in this study, the channels in both communities were assumed can carry flow with full depth. In addition, because the channels in both communities are natural channels with vegetation cover, Manning's Roughness Coefficient was assumed to be equal for both communities.

$$Q = \left(\frac{1.49}{n}\right) AR^{\frac{2}{3}}\sqrt{S} \quad (4\text{-}1)$$

Where:

Q = Flow Rate (ft^3/s)

n = Manning's Roughness Coefficient

R = Hydraulic Radius (ft) = A/WP

A = Flow cross-sectional area (ft^2)

WP = Wetted perimeter of flow (ft)

S = Channel longitudinal slope (ft/ft)

The channels in the Rockport community are significantly wider and have significantly flatter side slopes than those in the Sunnyside community (P-value < 0.01), indicating that the Rockport community has better channel width and side slopes. The cross-sectional areas of the channels in the Rockport community are significantly greater than that in the Sunnyside community, despite having significantly shallower depth. These results can be explained by the channel design requirements in the two communities. Aransas County has no specified minimum required channel depth and width; instead, it is calculated based on peak flow and the required minimum channel freeboard. For side slopes, Aransas County requires 1V:4H side slope, whereas Harris County requires 1V:3H side slope, explaining the flatter side slopes in the Rockport community.

The pipes/culverts density in the Rockport community is significantly lower than that in the Sunnyside community; however, the average pipes/culverts length in the Rockport community is significantly longer than that in the Sunnyside community. These

results can be explained by the fact that the housing density (houses per acre) in the Rockport community is less than that in the Sunnyside community.

Finally, there is no statistically significant difference between the two communities in terms of the longitudinal slope and channel capacity.

Table 4.8 ANOVA of channel condition attributes for the two studied communities.

Attribute	Sunnyside		Rockport		ANOVA P-Value	Significance[1]
	n	Median	n	Median		
Channel Depth, ft	20	1.62	19	1.34	4.61E-02	**
Bottom Width, ft	20	2.27	19	5.58	9.37E-08	***
Side Slope	40	0.312	38	0.186	1.11E-07	***
Avg. P/C Length, ft	20	11.98	19	23.55	1.06E-04	***
Longitudinal Slope	20	0.120%	19	0.093%	3.69E-01	
P/C Density	20	20.1%	19	15.9%	5.90E-03	***
Cross-sectional Area, ft^2	20	12.22	19	19.63	6.94E-06	***
Channel Capacity, ft^3/s	20	0.57/n[2]	19	0.84/n	1.87E-01	

[1] P<0.01: ***, P<0.05: **, P<0.1: *
[2] n: Manning's Roughness Coefficient

Table 4.9 and Figure 4.6 compare the off-channel drainage conditions in the two communities. The medians of OMEP and AFAA in the Rockport community are both less than that in the Sunnyside community. As discussed earlier, OMEP represents the percentage of major end points away from roadside channels, but it does not account for the accumulation of water in these end points. AFAA represents the actual average flow accumulation areas; thus is more critical in describing the potential for water ponding in the neighborhood. The Rockport community has three relatively large AFAA values, one of which is larger than three standard deviations (Figure 4.6). Thus, the off-channel

drainage condition in the Rockport community may lead to ponding issues and require the residents to take corrective actions and improvements to reduce the potential for water ponding on their properties.

Table 4.9 ANOVA of off-channel attributes for the two studied communities.

Attribute	Sunnyside		Rockport		ANOVA P-Value	Significance[(1)]
	n	Median	n	Median		
OMEP	10	27.50%	20	22.22%	7.84E-02	*
AFAA, sq. yard	10	124	20	111.5	7.08E-01	

[(1)] P<0.01: ***, P<0.05: **, P<0.1: *

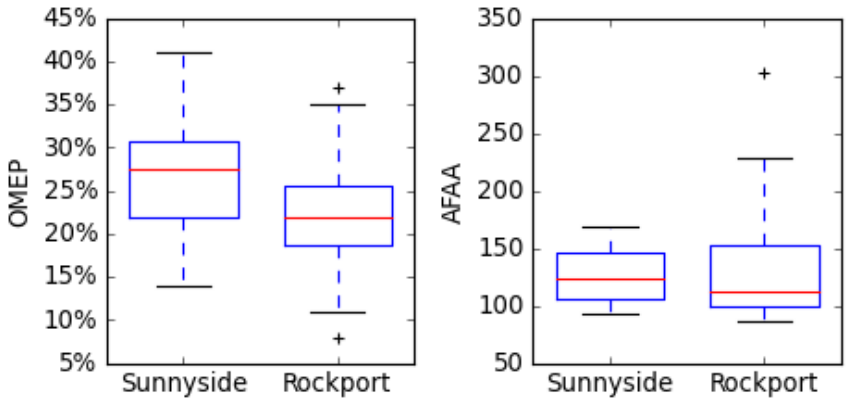

Figure 4.6 AFAA and OMEP comparisons between the two communities.

4.6. Conclusion

The drainage conditions of roadside channels and adjacent land were evaluated for two Texas communities that are vulnerable to flooding and stormwater-related hazards. The two case study communities are located in Harris county (Sunnyside community) and Aransas county (Rockport community), with a total street length of 4.67 centerline miles. These evaluations were performed based on using six geometrical attributes for channel

conditions and two attributes for off-channel conditions. The data for these attributes were obtained from mobile lidar.

The overall channel conditions in the Rockport community are generally better than those in the Sunnyside community. The channels in the Rockport community are significantly wider and have significantly flatter side slopes than those in the Sunnyside community. The cross-sectional areas of the channels in the Rockport community are significantly greater than that in the Sunnyside community, despite having significantly shallower depth. Since channel capacity depends on both cross-sectional area and longitudinal slope, there is no significant difference between these two communities in terms of channel capacity due to greater wetted perimeter of flow (and consequently smaller hydraulic radius) in the Rockport community. However, the median channel capacity in the Rockport community is 1.47 times that in the Sunnyside community. For off-channel drainage conditions, although the medians of OMEP and AFAA in the Rockport community are both less than that in the Sunnyside community, there are three relatively large AFAA values in the Rockport community that require improvement.

The differences in channel conditions between the two communities may be attributed to the intensity of the developed lands, the age of the communities, and variations in drainage design requirements. More than 80% of the developed lands in the Rockport community are low-intensity or open space, which enables the Rockport community to have more spaces for the channels. Additionally, the median "year structure built" indicates that the Rockport community is 16 years younger than the Sunnyside community; which may further explain the difference in drainage system condition; that

is the drainage system in Sunnyside is older and has been deteriorating over a longer service life. Finally, the case studies show that mobile lidar data can be used to evaluate drainage systems and provide actionable information to both property owners (to address potential off-channel ponding issues) and the municipal authorities (to address channel issues).

5. SUMMARY, CONCLUSIONS, AND RECOMMENDATIONS

5.1. Summary

Assessing drainage conditions at the neighborhood level can help public works agencies to develop maintenance plans and mitigation strategies to guard against pluvial floods. Drainage condition assessments can also inform property owners about possible drainage problem areas. Current drainage condition assessment methods have two common shortcomings: (a) they depend on manual visual inspection, which is a time-consuming and labor-intensive process, and (b) they ignore areas outside the street right-of-way (e.g., adjacent front yards), despite the interdependency between public drainage system (e.g., roadside channel) and adjacent private properties. To address these shortcomings, this dissertation aims to develop automated methods for assessing the drainage conditions of roadside channels and adjacent land in residential areas by using mobile lidar. Three different techniques, namely, semantic segmentation, flow direction determination, and cloth simulation filter algorithm, were introduced and incorporated in the first and second papers. Case studies were conducted in the third paper by applying the automated methods to assess the drainage conditions in two Texas communities that are socially and physically vulnerable to flooding and stormwater-related hazards.

First, this dissertation developed and provided an automated process for inspecting and evaluating roadside channel systems using data obtained from mobile lidar. The Cloth Simulation Filtering algorithm was employed to split lidar point clouds into bare earth and object datasets. Six key geometrical attributes of roadside channels were computed and analyzed based on the bare earth dataset using statistical and heuristic methods. These

geometrical attributes were compared to design and performance manuals to determine deficiencies and inform maintenance decisions. Second, roadside topography was modeled to evaluate surface drainage conditions by incorporating semantic segmentation and flow direction determination using mobile lidar data. The semantic segmentation model identifies the topographic features of lidar images by labeling each pixel as roadside channel, road, or adjacent land. Through the flow direction determination technique, major end points that are away from the roadside channels were identified as problematic low points that could be vulnerable to water ponding. Third, the developed methods were applied to two communities in Harris county (Sunnyside community) and Aransas county (Rockport community) in Texas, with a total street length of 4.67 centerline miles. The six geometrical attributes for channel conditions and two attributes for off-channel conditions were evaluated and compared in the case studies.

5.2. Conclusions

The dissertation shows that the proposed automated methods can effectively evaluate roadside channels and model the roadside topography within a street, providing an alternative to conventional manual inspection methods. The results benefit both property owners (to address potential off-channel ponding issues) and the public works agencies (to address channel issues) by providing crucial and actionable information at the street and neighborhood levels so that improvements can be implemented to mitigate against localized flooding and water ponding.

The specific conclusions of this dissertation are categorized according to the three papers and are shown in the following sections.

5.2.1. Paper 1: Automating the Evaluation of Urban Roadside Drainage Systems Using Mobile Lidar Data

- This paper developed an automated method to calculate six key roadside channel geometrical attributes reliably from raw lidar data. The six attributes are: channel depth, bottom width, side slope, longitudinal slope, and length and density of subsurface pipes and culverts.
- The developed automated process was applied to evaluate six street sections in the City of Houston. The analysis results show that every channel in the study site was found to have its own individual condition issues and improvement needs based on the requirements set by the City of Houston and Harris County.
- Mobile lidar can capture nearly continuous measurements along the channel; thus, the condition of drainage channels can be understood more comprehensively than manual inspection methods with random sampling.

5.2.2. Paper 2: Modeling Roadside Topography to Assess Drainage Conditions: A Computer Vision and Flow Direction Method Applied to Lidar Data

- The trained semantic segmentation model has the ability to identify key drainage and land features within a street block based on lidar images with intersection-over-union (IoU) and accuracy (ACC) of about 80.3% and 88.5% for the test dataset, respectively.
- Two off-channel attributes, off-channel major end points percentage (OMEP) and average flow accumulation area per off-channel major end point (AFAA), were developed and used to assess off-channel surface drainage conditions.

- In the test data set (10 street blocks in Houston and Rockport), three street blocks (#1, #2, and #9) had relatively high AFAA, indicating that a high water volume may not be conveyed to drainage channels appropriately.
- For one street block (#1), the OMEP was 47.2%, indicating that about half of the major end points in that street block were off-channels. These major end points may require additional maintenance to prevent water ponding and flooding issues. By contrast, on another street block (#7), all major end points were in or close to the roadside channels.
- One street block (#1) had the highest AFAA and OMEP among the test dataset, indicating that this street block needs additional maintenance to avoid water ponding and address potential localized flooding.
- Overall, the developed method shows that problematic low points within a street and its adjacent land can be identified by applying flow direction determination and considering proximity to roadside channels.

5.2.3. Paper 3: Use of Mobile Lidar for Assessing Drainage Conditions in Residential Areas with Roadside Channels: Case Studies

- The overall channel conditions in the Rockport community are generally better than those in the Sunnyside community.
- The cross-sectional areas of the channels in the Rockport community are significantly greater than that in the Sunnyside community. However, there is no significant difference between these two communities in terms of channel capacity

due to greater wetted perimeter of flow (and consequently smaller hydraulic radius) in the Rockport community.

- The medians of OMEP and AFAA in the Rockport community are both less than that in the Sunnyside community; however, there are three street blocks with relatively large AFAA values in the Rockport community that require improvement.
- Overall, the differences in channel conditions between the two communities may be attributed to the intensity of the developed lands, the age of the communities, and variations in drainage design requirements.

5.3. Recommendations

Further studies may be needed in the following areas:

- Develop a flood risk assessment method based on the output of the drainage condition assessment methods presented here.
- Investigate the advantages and disadvantages of land-based mobile lidar compared to airborne lidar for obtaining the data required by the developed methods.
- Expand the training dataset for the semantic segmentation algorithm to enhance its performance in identifying drainage infrastructures and adjacent land features within a street block.
- Integrate additional roadside channel condition information (e.g., blockages, erosion, etc.) into the developed methods to obtain a more comprehensive assessment of drainage conditions.

- Extend the developed methods to different drainage systems in residential and non-residential areas (e.g., areas with curb-and-gutter systems).
- Understand the relationship between social demographic and drainage conditions by applying the developed methods.

REFERENCES

Agency for Toxic Substances and Disease Registry. (2020). *CDC SVI 2018 Documentation*.

Aransas County. (2011). Aransas County Stormwater Management Plan. Retrieved from https://www.aransascounty.org/stormwatermgmt/e-docs/FINAL20110308%20Open%20House%20-%20AC%20SWMP.pdf accessed on

Aransas County. (2012). *Stormwater Master Plan and Guidance Manual: Development Guidelines & Stormwater Management Design Criteria for Aransas County*.

Aransas County. (2017a). Aransas County Multi-Jurisdictional Floodplain Management Plan Volume I. Retrieved from https://cityofrockport.com/ArchiveCenter/ViewFile/Item/1441 accessed on

Aransas County. (2017b). Aransas County Texas Multi-Jurisdictional Hazard Mitigation Action Plan. Retrieved from https://www.cityofrockport.com/ArchiveCenter/ViewFile/Item/2686

Arthur L. Storey, J. (1988). *Harris County Design Guidelines*. Harris County, Texas

Arthur L. Storey, J., & Freeman, J. L. (2005). *Regulations of Harris County, Texas for the Construction of Driveways and/or Culverts on County Easements and Rights-Of-Way*.

Atkinson, G. A., Zhang, W., Hansen, M. F., Holloway, M. L., & Napier, A. A. (2020). Image segmentation of underfloor scenes using a mask regions convolutional neural network with two-stage transfer learning. *Automation in Construction, 113*, 103118. doi:https://doi.org/10.1016/j.autcon.2020.103118

Badger, J. (2013). *Galveston County Drainage Design Requirements*. Galveston County

Badrinarayanan, V., Kendall, A., & Cipolla, R. (2017). SegNet: A Deep Convolutional Encoder-Decoder Architecture for Image Segmentation. *IEEE transactions on pattern analysis and machine intelligence, 39*(12), 2481-2495. doi:10.1109/TPAMI.2016.2644615

Bailly, J. S., Lagacherie, P., Millier, C., Puech, C., & Kosuth, P. (2008). Agrarian landscapes linear features detection from LiDAR: application to artificial drainage networks. *International Journal of Remote Sensing, 29*(12), 3489-3508. doi:10.1080/01431160701469057

Biesboer, D. D., & Elfering, J. (2003). Improving the Design of Roadside Ditches to Decrease Transportation-Related Surface Water Pollution. *Retrieved from the University of Minnesota Digital Conservancy, http://hdl.handle.net/11299/783*. Retrieved from http://hdl.handle.net/11299/783

Bolourian, N., & Hammad, A. (2020). LiDAR-equipped UAV path planning considering potential locations of defects for bridge inspection. *Automation in Construction, 117*, 103250. doi:https://doi.org/10.1016/j.autcon.2020.103250

Bonczak, B., & Kontokosta, C. E. (2019). Large-scale parameterization of 3D building morphology in complex urban landscapes using aerial LiDAR and city administrative data. *Computers, Environment and Urban Systems, 73*, 126-142. doi:https://doi.org/10.1016/j.compenvurbsys.2018.09.004

Brater, R. A. (2016). King County Road Design and Construction Standards.

Brubaker, A. (2020). Summit County Ditches - Roadside Drainage Brochure. Retrieved from https://www.summitengineer.net/files/12061/file/roadside-drainage_dk_070814.pdf accessed on May 23, 2020

Caesar, H., Uijlings, J., & Ferrari, V. (2018). *Coco-stuff: Thing and stuff classes in context.* Paper presented at the Proceedings of the IEEE Conference on Computer Vision and Pattern Recognition.

Cha, G., Park, S., & Oh, T. (2019). A Terrestrial LiDAR-Based Detection of Shape Deformation for Maintenance of Bridge Structures. *Journal of Construction Engineering and Management, 145*(12), 04019075. doi:doi:10.1061/(ASCE)CO.1943-7862.0001701

Cha, Y.-J., Choi, W., & Büyüköztürk, O. (2017). Deep Learning-Based Crack Damage Detection Using Convolutional Neural Networks. *Computer-Aided Civil and Infrastructure Engineering, 32*(5), 361-378. doi:10.1111/mice.12263

Chen, L., Papandreou, G., Kokkinos, I., Murphy, K., & Yuille, A. L. (2018). DeepLab: Semantic Image Segmentation with Deep Convolutional Nets, Atrous Convolution, and Fully Connected CRFs. *IEEE transactions on pattern analysis and machine intelligence, 40*(4), 834-848. doi:10.1109/TPAMI.2017.2699184

Chen, L.-C., Papandreou, G., Schroff, F., & Adam, H. (2017). Rethinking atrous convolution for semantic image segmentation. *arXiv preprint arXiv:1706.05587*.

Chin, A., & Olsen, M. J. (2015). Evaluation of Technologies for Road Profile Capture, Analysis, and Evaluation. *Journal of Surveying Engineering, 141*(1), 04014011. doi:doi:10.1061/(ASCE)SU.1943-5428.0000134

Chou, C.-P., Lee, C.-C., Chen, A.-C., & Wu, C.-Y. (2017). Using a constructive pavement texture index for skid resistance screening. *International Journal of Pavement Research and Technology, 10*(4), 360-368. doi:https://doi.org/10.1016/j.ijprt.2017.05.002

City and County of Honolulu Department of Planning and Permitting. (2000). *Rules Relating to Storm Drainage Standards*.

City of Charlotte. (2013). *City of Charlotte Driveway Regulations*.

City of Charlotte. (2014). *Charlotte-Mecklenburg Storm Water Design Manual*.

City of Fairfax. (2017). *Public Facilities Manual*.

City of Houston. (2018). Hazard Mitigation Plan Update. Retrieved from https://s3-us-west-2.amazonaws.com/uasi-jtti/wp-content/uploads/sites/29/2019/11/15165319/City_of_Houston_HMAP_Updated_0723191.pdf accessed on

City of Tulsa. (2017). *Tulsa City Stormwater Management Criteria Manual*

Clark County. (1999). *Regional Flood Control District Hydrologic Criteria and Drainage Design Manual - Section 700 Open Channels*

Cook County. (2012). *Cook County Drainage Design Criteria*.

Cook County. (2020). *Part II - Land Development Ordinances Chapter 102 - Buildings And Building Regulations*.

Cordts, M., Omran, M., Ramos, S., Rehfeld, T., Enzweiler, M., Benenson, R., Franke, U., Roth, S., & Schiele, B. (2016). *The cityscapes dataset for semantic urban scene understanding.* Paper presented at the Proceedings of the IEEE conference on computer vision and pattern recognition.

Czerniawski, T., & Leite, F. (2019). Semantic Segmentation of Building Point Clouds Using Deep Learning: A Method for Creating Training Data Using BIM to Point Cloud Label Transfer. In *Computing in Civil Engineering 2019* (pp. 410-416).

Douglas County. (2008). *Douglas County Storm Drainage Design and Technical Criteria Manual*.

Douglas County. (2015). *Typical Driveway Construction Per Douglas County Regulations and Policies*

Dung, C. V., & Anh, L. D. (2019). Autonomous concrete crack detection using deep fully convolutional neural network. *Automation in Construction, 99*, 52-58. doi:https://doi.org/10.1016/j.autcon.2018.11.028

Ellis, J. B., Viavattene, C., Chlebek, J., & Hetherington, D. (2012). Integrated modelling for urban surface water exceedance flows. *Proceedings of the Institution of Civil Engineers - Water Management, 165*(10), 543-552. doi:10.1680/wama.12.00029

Ellis, K., Berg, C., Caraco, D., Drescher, S., Hoffmann, G., Keppler, B., LaRocco, M., & A.Turner. (2014). Low Impact Development in Coastal South Carolina: A Planning and Design Guide. *ACE Basin and North Inlet – Winyah Bay National Estuarine Research Reserves*.

Ettrich, N., Steiner, K., Thomas, M., & Rothe, R. (2005). Surface models for coupled modelling of runoff and sewer flow in urban areas. *Water Science and Technology, 52*(5), 25-33. doi:10.2166/wst.2005.0101

FEMA – OpenFEMA Dataset: Individual Assistance Housing Registrants Large Disasters – V1. (2019). Retrieved from https://www.fema.gov/openfema-dataset-individual-assistance-housing-registrants-large-disasters-v1 accessed on July 10, 2020

Flanagan, B. E., Gregory, E. W., Hallisey, E. J., Heitgerd, J. L., & Lewis, B. (2011). A Social Vulnerability Index for Disaster Management. *Journal of Homeland Security and Emergency Management, 8*(1), 000010220215477355179 2. doi:https://doi.org/10.2202/1547-7355.1792

Fort Wayne City. (2017). *City Utilities Design Standards Manual*.

Frank, J. E., & Falconer, M. K. (1990). The measurement of infrastructure capacity: Theory, data structures, and analytics. *Computers, Environment and Urban Systems, 14*(4), 283-297. doi:https://doi.org/10.1016/0198-9715(90)90003-C

Gao, C., & Elzarka, H. (2021). The use of decision tree based predictive models for improving the culvert inspection process. *Advanced Engineering Informatics, 47*, 101203. doi:https://doi.org/10.1016/j.aei.2020.101203

Garcia-Garcia, A., Orts-Escolano, S., Oprea, S., Villena-Martinez, V., & Garcia-Rodriguez, J. (2017). A review on deep learning techniques applied to semantic segmentation. *arXiv preprint arXiv:1704.06857*.

Gargoum, S. A., Karsten, L., El-Basyouny, K., & Koch, J. C. (2018). Automated assessment of vertical clearance on highways scanned using mobile LiDAR technology. *Automation in Construction, 95*, 260-274. doi:https://doi.org/10.1016/j.autcon.2018.08.015

GIMS – GIM Public. (2020). Retrieved from http://www.gims.houstontx.gov/gims/default.aspx?app_id=gims&app=GIMS&AppID=-1&app=GIMS accessed on July 10, 2020

GIMS – Public Utility Map. (2020). Retrieved from http://www.gims.houstontx.gov/PublicUtilityMap/ accessed on July 10, 2020

Gopalakrishnan, K., Khaitan, S. K., Choudhary, A., & Agrawal, A. (2017). Deep Convolutional Neural Networks with transfer learning for computer vision-based data-driven pavement distress detection. *Construction and Building Materials, 157*, 322-330. doi:https://doi.org/10.1016/j.conbuildmat.2017.09.110

Gurganus, C. F., Gharaibeh, N. G., & Scullion, T. (2017). Case Study on the Use of Mobile Lidar to Produce a Preliminary Drainage Design. *Transportation Research Record, 2655*(1), 82-90. doi:10.3141/2655-11

Hackl, J., Adey, B. T., & Lethanh, N. (2018). Determination of Near-Optimal Restoration Programs for Transportation Networks Following Natural Hazard Events Using Simulated Annealing. *Computer-Aided Civil and Infrastructure Engineering, 33*(8), 618-637. doi:10.1111/mice.12346

Hackl, J., Adey, B. T., Woźniak, M., & Schümperlin, O. (2018). Use of Unmanned Aerial Vehicle Photogrammetry to Obtain Topographical Information to Improve Bridge Risk Assessment. *Journal of Infrastructure Systems, 24*(1), 04017041. doi:doi:10.1061/(ASCE)IS.1943-555X.0000393

Haddock, C. E., & Myers, J. T. (2018). Houston Public Works, Infrastructure Design Manual.

Harris County Flood Control Districts – Flood Education Mapping Tool. (2020). Retrieved from https://www.harriscountyfemt.org/ accessed on July 10, 2020

Haubner, S., Reese, A., Brown, T., Claytor, R., & Debo, T. (2001). *Georgia Stormwater Management Manual Volume 2: Technical Handbook*.

Hillsborough County. (2015). *Hillsborough County Stormwater Management Technical Manual*.

Hoffmann, G., Stack, R. C., & Wye, B. V. (2012). *District of Columbia Stromwater Management Guidebook*.

Jefferson County Planning and Zoning Division. (2019). *Jefferson County Storm Drainage Design & Technical Criteria*.

Kalfarisi, R., Wu, Z. Y., & Soh, K. (2020). Crack Detection and Segmentation Using Deep Learning with 3D Reality Mesh Model for Quantitative Assessment and Integrated Visualization. *Journal of Computing in Civil Engineering, 34*(3), 04020010. doi:doi:10.1061/(ASCE)CP.1943-5487.0000890

Kim, B., & Cho, S. (2019). Image-based concrete crack assessment using mask and region-based convolutional neural network. *Structural Control and Health Monitoring, 26*(8), e2381. doi:10.1002/stc.2381

Kim, W., & Seok, J. (2018, 3-6 July 2018). *Indoor Semantic Segmentation for Robot Navigating on Mobile.* Paper presented at the 2018 Tenth International Conference on Ubiquitous and Future Networks (ICUFN).

Kirillov, A., Girshick, R., He, K., & Dollár, P. (2019). *Panoptic feature pyramid networks.* Paper presented at the Proceedings of the IEEE Conference on Computer Vision and Pattern Recognition.

Koch, C., Georgieva, K., Kasireddy, V., Akinci, B., & Fieguth, P. (2015). A review on computer vision based defect detection and condition assessment of concrete and asphalt civil infrastructure. *Advanced Engineering Informatics, 29*(2), 196-210. doi:https://doi.org/10.1016/j.aei.2015.01.008

Krizhevsky, A., Sutskever, I., & Hinton, G. E. (2012). *Imagenet classification with deep convolutional neural networks.* Paper presented at the Advances in neural information processing systems.

Labelbox. (2020). Labelbox. Retrieved from https://labelbox.com accessed on May 24, 2020

Lee, C.-C., & Gharaibeh, N. G. (2020). Automating the evaluation of urban roadside drainage systems using mobile lidar data. *Computers, Environment and Urban Systems, 82*, 101502. doi:https://doi.org/10.1016/j.compenvurbsys.2020.101502

Lee, C.-C., & Gharaibeh, N. G. (2021). *Assessing Surface Drainage Conditions in Residential Areas Using Semantic Segmentation and Mobile Lidar Data*. Paper presented at the Transportation Research Board 100th Annual Meeting, Washington, D.C.

Lin, G., Milan, A., Shen, C., & Reid, I. (2017). *Refinenet: Multi-path refinement networks for high-resolution semantic segmentation.* Paper presented at the Proceedings of the IEEE conference on computer vision and pattern recognition.

Lincoln County. (2000). *Drainage Criteria Manual - Chapter 5: Open Channels*.

Long, J., Shelhamer, E., & Darrell, T. (2015). *Fully convolutional networks for semantic segmentation.* Paper presented at the Proceedings of the IEEE conference on computer vision and pattern recognition.

Maeda, H., Sekimoto, Y., Seto, T., Kashiyama, T., & Omata, H. (2018). Road damage detection using deep neural networks with images captured through a smartphone. *arXiv preprint arXiv:1801.09454*.

Manning, R. (1891). On the flow of water in open channels and pipes. *Transactions of the Institution of Civil Engineers of Ireland, 20*, 161-207.

Marion County Public Works. (1990). *Marion County Engineering Standards*.

Marion County Public Works. (2012). *Marion County Engineering Standards - Draft Interim Stormwater Quality Treatment Engineering Standards for the Storm Water Management Area*.

Molzahn, R. E., & Burke, C. B. (1986). Assessment of drainage infrastructure for urban areas. *Tunnelling and Underground Space Technology, 1*(3), 387-389. doi:https://doi.org/10.1016/0886-7798(86)90022-2

MRLC (Multi-Resolution Land Characteristic Consortium) – NLCD (National Land Cover Database) 2016 Land Cover (CONUS). (2019). Retrieved from https://www.mrlc.gov/data/nlcd-2016-land-cover-conus accessed on July 10, 2020

Nath, N. D., & Behzadan, A. H. (2019). Deep Learning Models for Content-Based Retrieval of Construction Visual Data. In *Computing in Civil Engineering 2019* (pp. 66-73).

Neupane, S. R., & Gharaibeh, N. G. (2019). A heuristics-based method for obtaining road surface type information from mobile lidar for use in network-level infrastructure management. *Measurement, 131*, 664-670. doi:https://doi.org/10.1016/j.measurement.2018.09.015

New York State. (2001). *New York State Stormwater Management Design Manual*.

New York State. (2008). *State of New York Department of Transportation Driveway Design Guidelines*.

NOAA – South Texas Heavy Rainfall - September 2-16, 2018. (2020). Retrieved from https://www.weather.gov/crp/september_2018_heavy_rain accessed on July 19, 2020

O'Callaghan, J. F., & Mark, D. M. (1984). The extraction of drainage networks from digital elevation data. *Computer Vision, Graphics, and Image Processing, 28*(3), 323-344. doi:https://doi.org/10.1016/S0734-189X(84)80011-0

Oklahoma Department of Transportation. (1992). *Roadway Design Manual*.

Oliveira, H., & Correia, P. L. (2009, 24-28 Aug. 2009). *Automatic road crack segmentation using entropy and image dynamic thresholding.* Paper presented at the 2009 17th European Signal Processing Conference.

Oti, I. C., Gharaibeh, N. G., Hendricks, M. D., Meyer, M. A., Zandt, S. V., Masterson, J., Horney, J. A., & Berke, P. (2019). Validity and Reliability of Drainage Infrastructure Monitoring Data Obtained from Citizen Scientists. *Journal of Infrastructure Systems, 25*(3), 04019018. doi:doi:10.1061/(ASCE)IS.1943-555X.0000495

Park, Y., & Guldmann, J.-M. (2019). Creating 3D city models with building footprints and LIDAR point cloud classification: A machine learning approach. *Computers, Environment and Urban Systems, 75*, 76-89. doi:https://doi.org/10.1016/j.compenvurbsys.2019.01.004

Passalacqua, P., Belmont, P., & Foufoula-Georgiou, E. (2012). Automatic geomorphic feature extraction from lidar in flat and engineered landscapes. *Water Resources Research, 48*(3). doi:10.1029/2011wr010958

Qi, J. (2020). CSF. *GitHub repository.* Retrieved from https://github.com/jianboqi/CSF accessed on Mar 05, 2020

Qin, C., Zhu, A. X., Pei, T., Li, B., Zhou, C., & Yang, L. (2007). An adaptive approach to selecting a flow-partition exponent for a multiple-flow-direction algorithm. *International Journal of Geographical Information Science, 21*(4), 443-458. doi:10.1080/13658810601073240

Quinn, P. F., Beven, K., Chevallier, P., & Planchon, O. (1991). The prediction of hillslope flow paths for distributed hydrological modelling using digital terrain models. *Hydrological Processes, 5*(1), 59-79. doi:10.1002/hyp.3360050106

Quinn, P. F., Beven, K. J., & Lamb, R. (1995). The in(a/tan/β) index: How to calculate it and how to use it within the topmodel framework. *Hydrological Processes, 9*(2), 161-182. doi:10.1002/hyp.3360090204

Rhode Island State. (2010). *Rhode Island Stormwater Design and Installation Standards Manual*

Rice University's Baker Institute for Public Policy. (2019). Sunnyside and South Park Comprehensive Needs Assessment Data Report. Retrieved from https://www.bakerinstitute.org/media/files/research-document/5e17d4a1/chb-pub-sunnyside-110819.pdf accessed on

Ronneberger, O., Fischer, P., & Brox, T. (2015). *U-net: Convolutional networks for biomedical image segmentation.* Paper presented at the International Conference on Medical image computing and computer-assisted intervention.

San Diego County. (2005). *San Diego County Drainage Design Manual*.

Schwanghart, W., & Scherler, D. (2014). Short Communication: TopoToolbox 2 – MATLAB-based software for topographic analysis and modeling in Earth surface sciences. *Earth Surf. Dynam., 2*(1), 1-7. doi:10.5194/esurf-2-1-2014

Seibert, J., & McGlynn, B. L. (2007). A new triangular multiple flow direction algorithm for computing upslope areas from gridded digital elevation models. *Water Resources Research, 43*(4). doi:10.1029/2006wr005128

Service, N. R. C. (2008). Chapter 5 Open Ditches for Drainage--Design, Construction, and Maintenance. In *National engineering handbook, Part 624 - Drainage (Water Table Control), Section 16 drainage of agricultural land*. Washington, D.C.: Natural Resources Conservation Service.

State of Georgia Department of Transportation. (2019). Regulations for Driveway and Encroachment Control.

Tanoue, D. K. (2011). *Driveway Apron Guidelines for Unimproved Sidewalk Areas*.

Tarboton, D. G. (1997). A new method for the determination of flow directions and upslope areas in grid digital elevation models. *Water Resources Research, 33*(2), 309-319. doi:10.1029/96wr03137

Tregoning, H., & Bellamy, T. (2019). District of Columbia Public Realm Design Manual.

Tsai, Y.-C., & Chatterjee, A. (2018). Pothole Detection and Classification Using 3D Technology and Watershed Method. *Journal of Computing in Civil Engineering, 32*(2), 04017078. doi:doi:10.1061/(ASCE)CP.1943-5487.0000726

U.S. Census – 2014-2018 ACS (American Community Survey) 5-year Data Profile. (2019). Retrieved from https://www.census.gov/acs/www/data/data-tables-and-tools/data-profiles/ accessed on July 10, 2020

U.S. Census – 2018 ACS (American Community Survey) 5-year Estimates. (2019). Retrieved from https://www2.census.gov/programs-surveys/acs/summary_file/2018/data/ accessed on July 10, 2020

W. Zhang, J. Qi, P. Wan, H. Wang, D. Xie, X. Wang, & Yan, G. (2020). CSF. Retrieved from http://ramm.bnu.edu.cn/projects/CSF/ accessed on Mar 05, 2020

Wang, Y.-J., Qin, C.-Z., & Zhu, A. X. (2019). Review on algorithms of dealing with depressions in grid DEM. *Annals of GIS, 25*(2), 83-97. doi:10.1080/19475683.2019.1604571

Weil, J. (1986). The synthesis of cloth objects. *SIGGRAPH Comput. Graph., 20*(4), 49-54. doi:10.1145/15886.15891

Wilson, J. P. (2018). Calculating Land Surface Parameters. In *Environmental Applications of Digital Terrain Modeling* (pp. 53-149): John Wiley & Sons.

Wu, H., Zhang, J., Huang, K., Liang, K., & Yu, Y. (2019). FastFCN: Rethinking dilated convolution in the backbone for semantic segmentation. *arXiv preprint arXiv:1903.11816*.

Wu, Y., Kirillov, A., Massa, F., Lo, W.-Y., & Girshick, R. (2019). Detectron2. *GitHub repository.* Retrieved from https://github.com/facebookresearch/detectron2 accessed on May 24, 2020

Xu, G., Huang, G. Q., & Fang, J. (2015). Cloud asset for urban flood control. *Advanced Engineering Informatics, 29*(3), 355-365. doi:https://doi.org/10.1016/j.aei.2015.01.006

Yu, F., & Koltun, V. (2015). Multi-scale context aggregation by dilated convolutions. *arXiv preprint arXiv:1511.07122*.

Zhang, K., Cheng, H. D., & Zhang, B. (2018). Unified Approach to Pavement Crack and Sealed Crack Detection Using Preclassification Based on Transfer Learning. *Journal of Computing in Civil Engineering, 32*(2), 04018001. doi:doi:10.1061/(ASCE)CP.1943-5487.0000736

Zhang, W., Li, W., Zhang, C., Hanink, D. M., Li, X., & Wang, W. (2017). Parcel-based urban land use classification in megacity using airborne LiDAR, high resolution orthoimagery, and Google Street View. *Computers, Environment and Urban Systems, 64*, 215-228. doi:https://doi.org/10.1016/j.compenvurbsys.2017.03.001

Zhang, W., Qi, J., Wan, P., Wang, H., Xie, D., Wang, X., & Yan, G. (2016). An Easy-to-Use Airborne LiDAR Data Filtering Method Based on Cloth Simulation. *Remote Sensing, 8*(6), 501. doi:ARTN 501 10.3390/rs8060501

Zhang, X., Rajan, D., & Story, B. (2019). Concrete crack detection using context-aware deep semantic segmentation network. *Computer-Aided Civil and Infrastructure Engineering, 34*(11), 951-971. doi:10.1111/mice.12477

Zhao, H., Shi, J., Qi, X., Wang, X., & Jia, J. (2017). *Pyramid scene parsing network.* Paper presented at the Proceedings of the IEEE conference on computer vision and pattern recognition.

Zhou, Z., & Gong, J. (2018). Automated residential building detection from airborne LiDAR data with deep neural networks. *Advanced Engineering Informatics, 36*, 229-241. doi:https://doi.org/10.1016/j.aei.2018.04.002

APPENDIX A

FLOWCHARTS FOR CHANNEL ATTRIBUTE CALCULATIONS

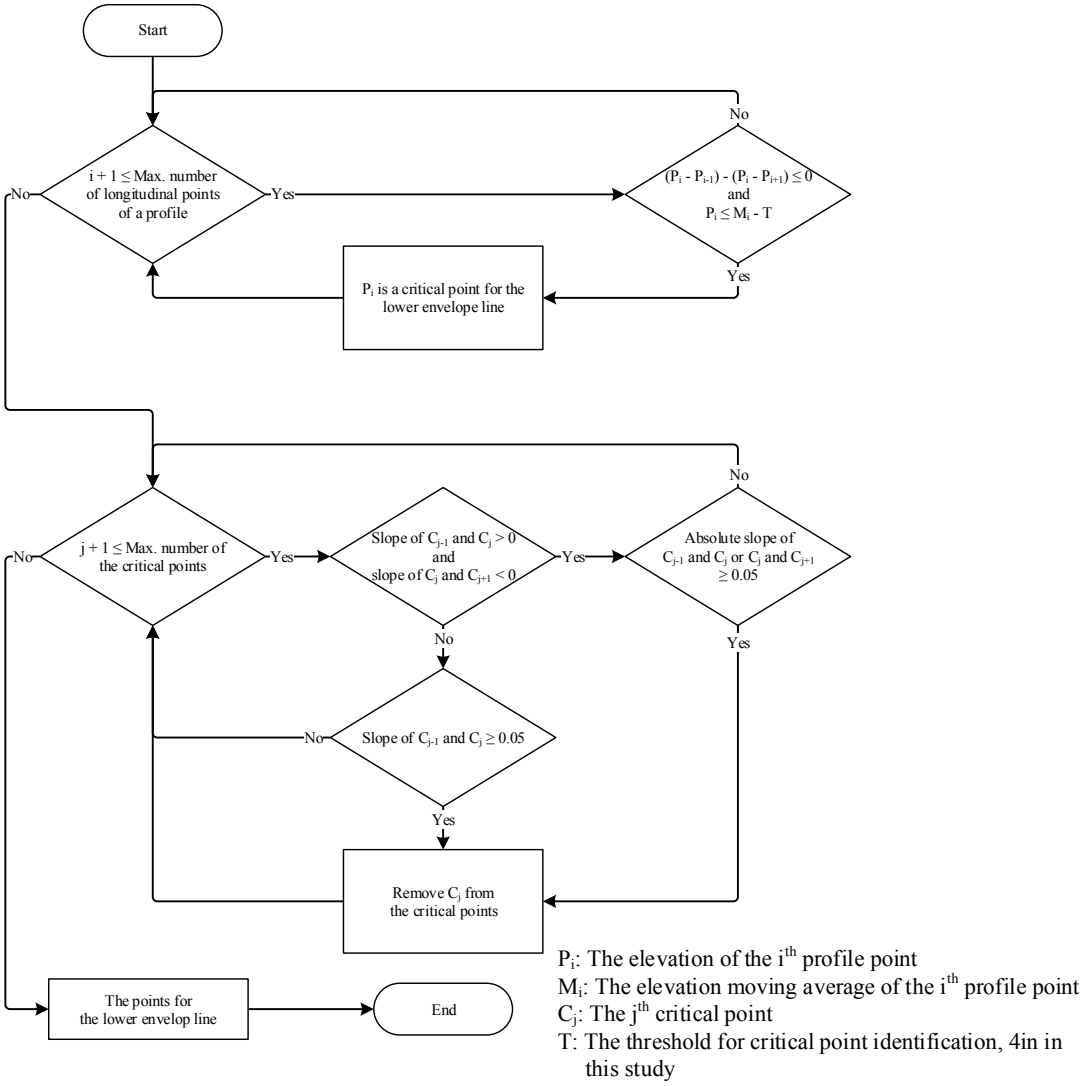

Figure A. 1 Data processing flowchart for generating the lower envelope line

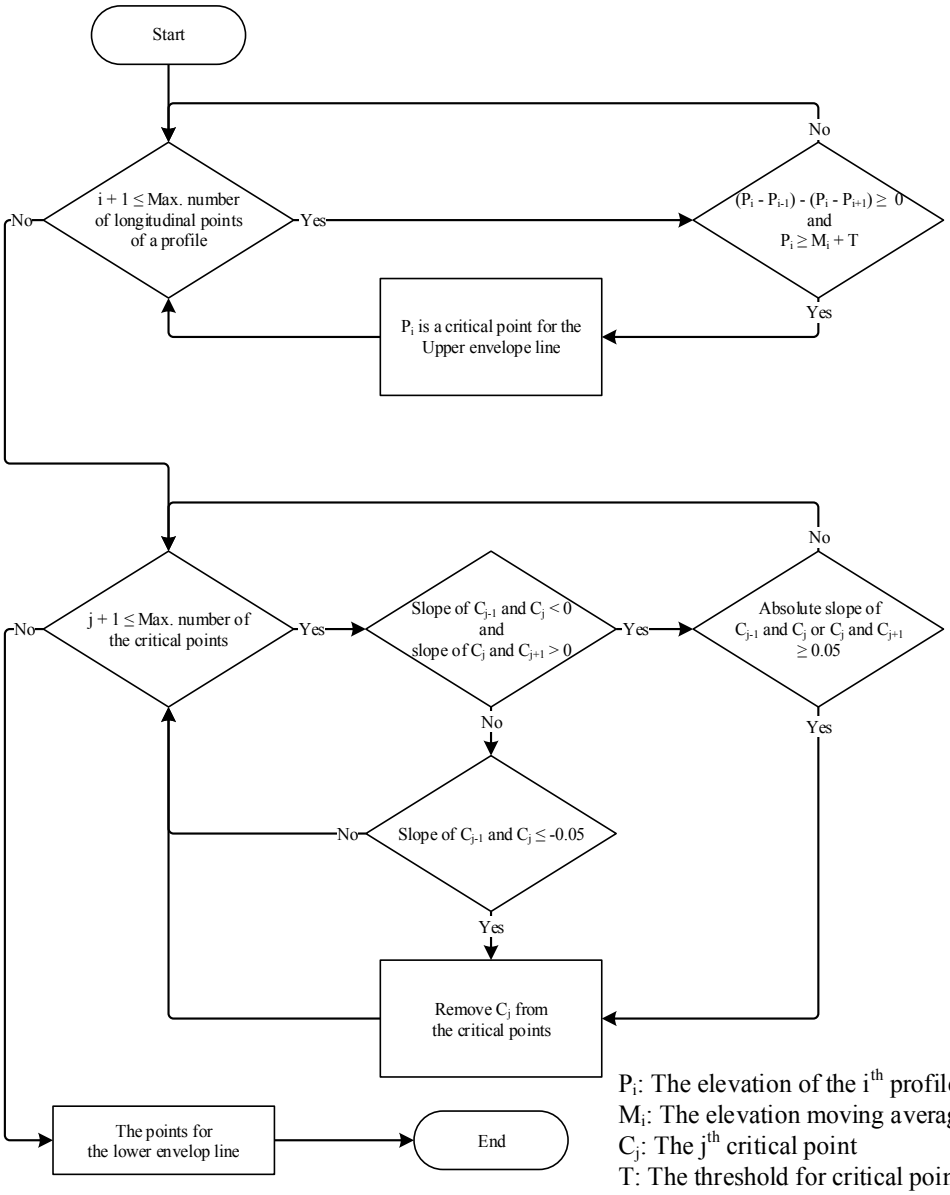

P_i: The elevation of the i^{th} profile point
M_i: The elevation moving average of the i^{th} profile point
C_j: The j^{th} critical point
T: The threshold for critical point identification, 4in in this study

Figure A. 2 Data processing flowchart for generating the upper envelope line

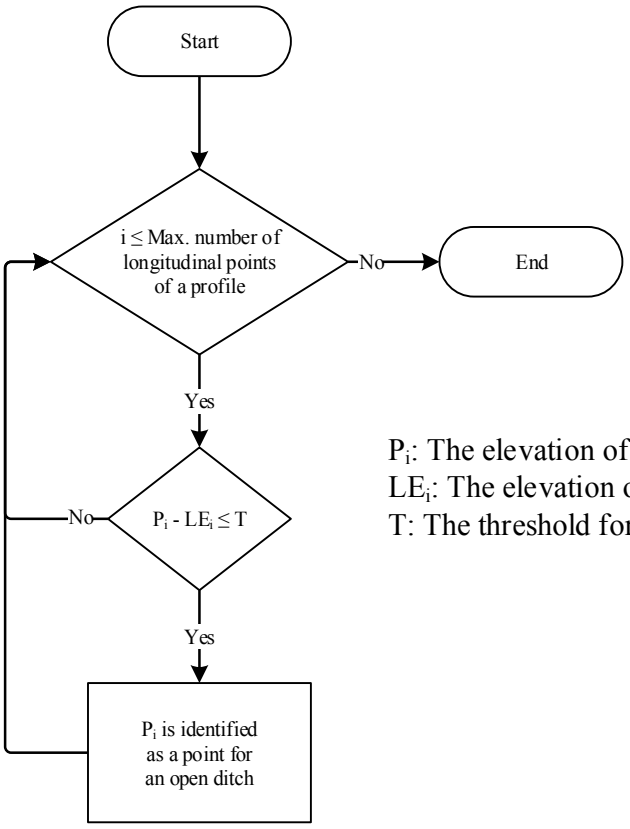

P_i: The elevation of the i^{th} profile point
LE_i: The elevation of the i^{th} lower envelope line point
T: The threshold for open ditch identification, 4in in this study

Figure A. 3 Data processing flowchart for identifying existence of open roadside channels

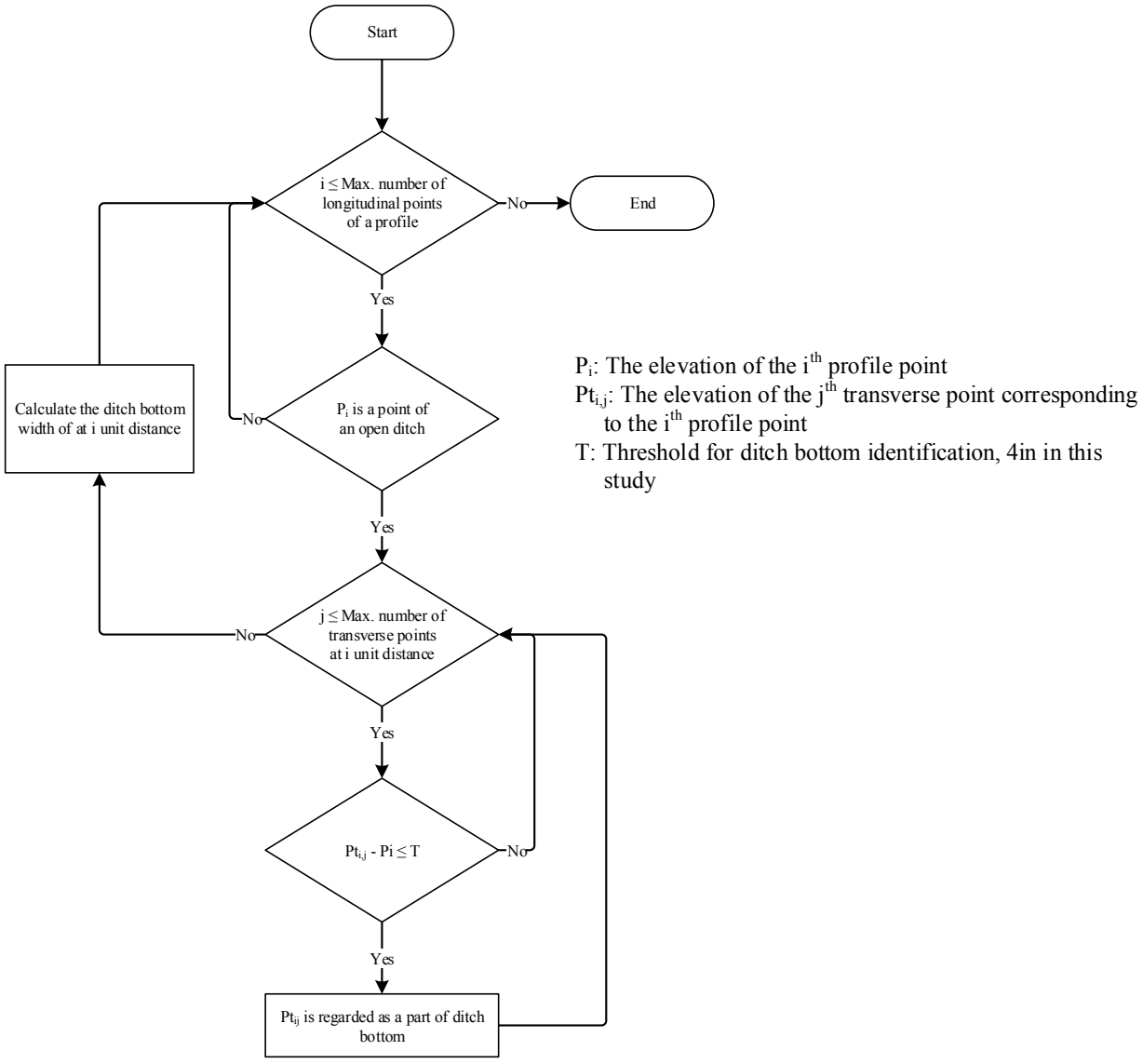

Figure A. 4 Data processing flowchart for calculating channel bottom width

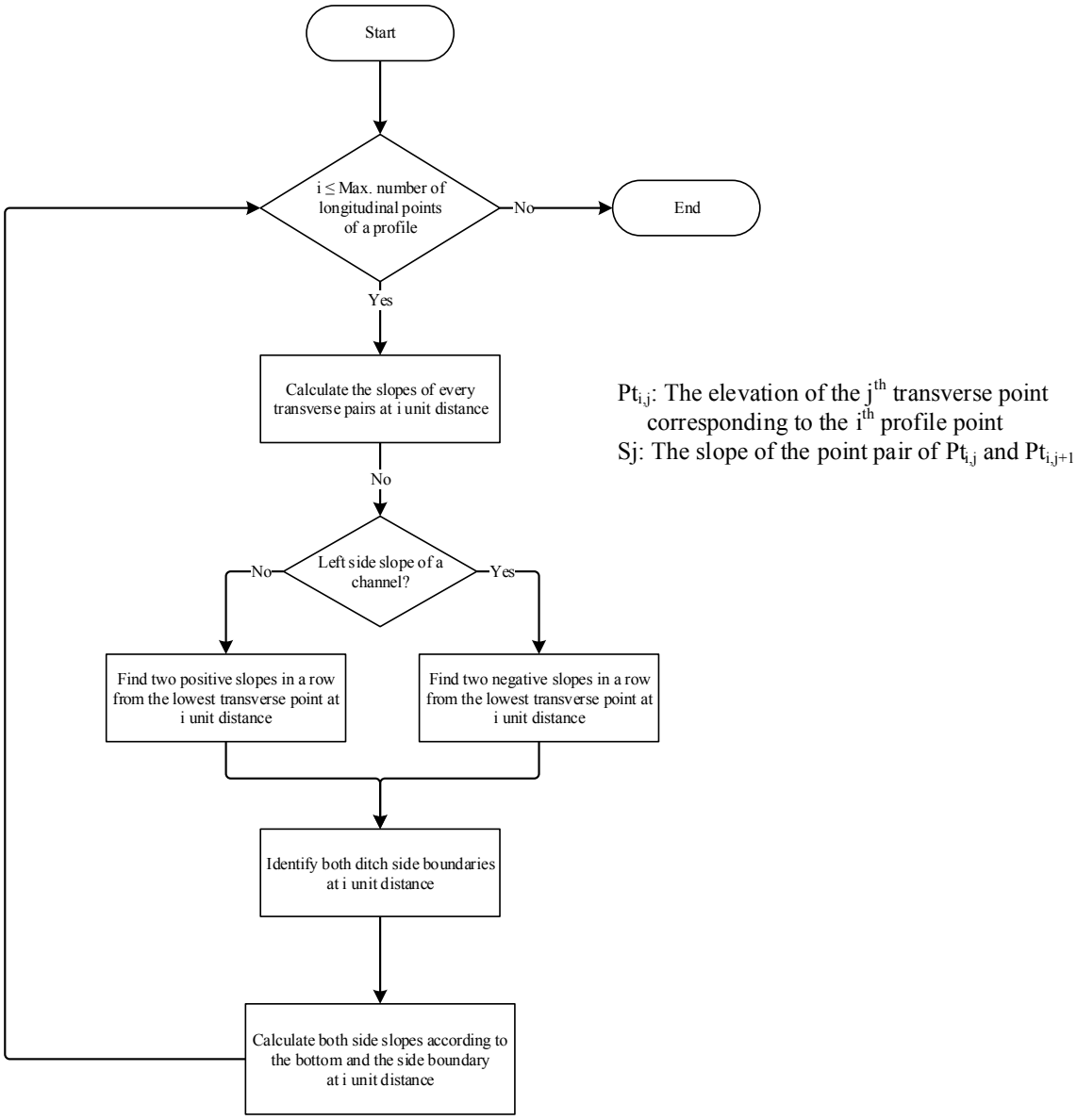

Figure A. 5 Data processing flowchart for calculating channel side slope

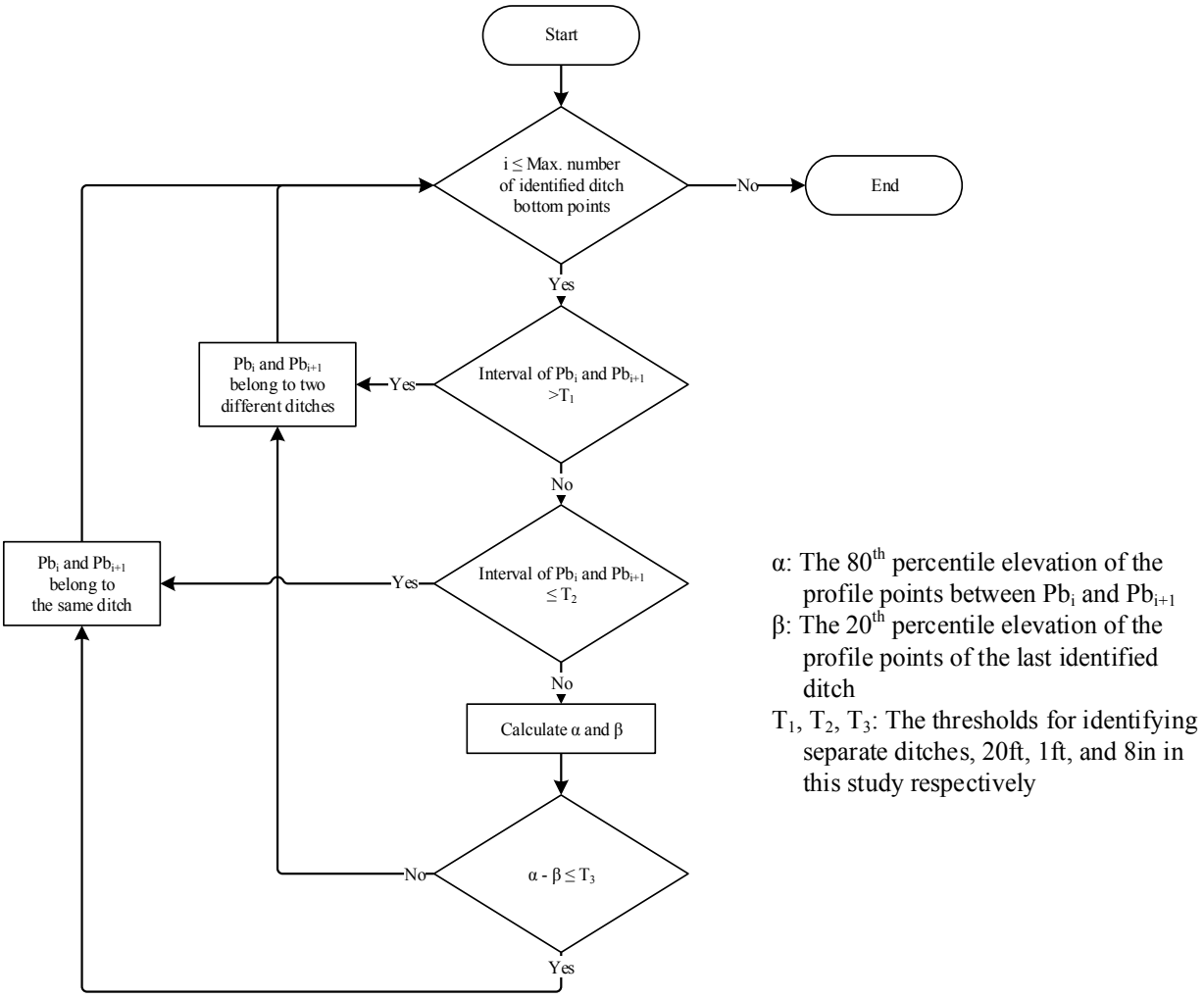

Figure A. 6 Data processing flowchart for calculating length and density of subsurface pipes and culverts